HHS Public Access

Author manuscript

Sci Immunol. Author manuscript; available in PMC 2024 October 21.

Published in final edited form as:

Sci Immunol. 2024 September 20; 9(99): eadl3755. doi:10.1126/sciimmunol.adl3755.

Two-dose priming immunization amplifies humoral immunity by synchronizing vaccine delivery with the germinal center response

Sachin H. Bhagchandani[1,2,3,5,7,†], **Leerang Yang**[1,4,6,7,†], **Jonathan H. Lam**[5], **Laura Maiorino**[2,5,8], **Elana Ben-Akiva**[2,5], **Kristen A. Rodrigues**[2,5], **Anna Romanov**[2,5], **Heikyung Suh**[5,8], **Aereas Aung**[2,5], **Shengwei Wu**[5], **Anika Wadhera**[2,5], **Arup K. Chakraborty**[1,3,4,6,7], **Darrell J. Irvine**[1,2,5,7,8]

[1]Department of Chemical Engineering, Massachusetts Institute of Technology, 77 Massachusetts Avenue, Cambridge, MA 02139, U.S.A.

[2]Department of Biological Engineering, Massachusetts Institute of Technology, 77 Massachusetts Avenue, Cambridge, MA 02139, U.S.A.

[3]Department of Chemistry, Massachusetts Institute of Technology, 77 Massachusetts Avenue, Cambridge, MA 02139, U.S.A.

[4]Department of Physics, Massachusetts Institute of Technology, 77 Massachusetts Avenue, Cambridge, MA 02139, U.S.A.

[5]Koch Institute for Integrative Cancer Research, Massachusetts Institute of Technology, 500 Main Street, Cambridge, MA 02139, U.S.A.

[6]Institute for Medical Engineering and Science, Massachusetts Institute of Technology, 77 Massachusetts Avenue, Cambridge, MA 02139, U.S.A.

[7]Ragon Institute of MGH, MIT, and Harvard, Cambridge, MA 02139, U.S.A.

[8]Howard Hughes Medical Institute, Chevy Chase, MD 20815, USA

Abstract

Prolonging exposure to subunit vaccines during the primary immune response enhances humoral immunity. Escalating-dose immunization (EDI), administering vaccines every other day in an increasing pattern over 2 weeks, is particularly effective but challenging to implement clinically.

*Correspondence to: djirvine@mit.edu & arupc@mit.edu.

†Denotes equal contributions

Author contributions: S.H.B, D.J.I, A.K,C and L.Y conceived the experiments and computational modeling framework, wrote the manuscript together and all authors discussed and commented on it. S.H.B, J.H.L, L.M, E.B.A, K.A.R, A.M.R, H.S, A.A, S.W, and A.W. performed all the experimental work and analyzed the data. L.Y. performed all the computational work, and interpreted them with A.K.C, S.H.B. and D.J.I.. S.H.B and L.Y generated the figures. D.J.I and A.K.C acquired funding and supervised the research.

Competing interests: For completeness, it is noted that A.K.C. is a consultant (titled "Academic Partner") for Flagship Pioneering, consultant and Member of the Board of Directors of its affiliated company, Apriori Bio, and is a consultant and Scientific Advisory Board Member of another affiliated company, Metaphore Bio.

Data and materials availability: The MATLAB scripts and instructions to reproduce the results can be found on our Zenodo repository at: zenodo.org/doi/10.5281/zenodo.12595649. All other data needed to support the conclusions of the paper are present in the paper or the Supplementary materials (see Data file S1).

Here, using an HIV Env trimer/saponin adjuvant vaccine, we explored simplified EDI regimens, and found that a two-shot regimen administering 20% of the vaccine followed by the remaining 80% of the dose 7 days later increased Tfh responses 5-fold, antigen-specific GC B cells 10-fold, and serum antibody titers 10-fold compared to bolus immunization. Computational modeling of Tfh priming and the GC response suggested that enhanced activation/antigen loading on dendritic cells as well as increased capture of antigen delivered in the second dose by follicular dendritic cells contribute to these effects, predictions we verified experimentally. These results suggest that a two-shot priming approach can be used to substantially enhance responses to subunit vaccines.

One-sentence summary :

Vaccine delivery in two doses, synchronized to germinal center dynamics and T cell priming, enhances humoral immunity.

INTRODUCTION

Vaccines are a critical public health tool for the control of infectious diseases as illustrated by their efficacy in mitigating morbidity and mortality during the COVID-19 pandemic (1). However, despite many advances, there remain a number of pathogens, including the human immunodeficiency virus (HIV), for which effective vaccines are unavailable, owing to challenges such as high mutation rates, immune evasion mechanisms, and unfavorable immunodominance patterns (2, 3). HIV continues to pose a persistent global health threat, and the development of an effective vaccine against the virus remains an urgent priority (4). Based on non-human primate and human studies of antibody passive transfer, a vaccine capable of eliciting broadly neutralizing antibodies (bnAbs) targeting conserved regions of the envelope spike (Env) that can neutralize diverse HIV strains should be protective against HIV infection (5-7). However, generation of antibodies capable of broad and potent native HIV neutralization via vaccination has proven challenging due to multiple factors including immunodominance of non-neutralizing epitopes, high sequence variability of the trimer, and limited structural accessibility of highly conserved epitopes (3, 8, 9). Similar challenges have hindered the development of universal influenza vaccines that target the relatively conserved receptor binding site of hemagglutinin (HA) (10, 11).

Following vaccination, germinal centers (GCs) play a pivotal role in the evolution of the clonality and affinity of the antibody response, and influence the composition of the memory B cell and long-lived plasma cell compartments following immunization (12, 13). The provision of antigen to GC B cells by follicular dendritic cells (FDCs), which efficiently capture complement- or antibody-decorated antigen, and support from follicular helper T cells (Tfh), which control GC B cell survival, are crucial factors in this process (14, 15). Notably, the size of the early GC response correlates with the magnitude of neutralizing antibodies (Abs) generated by immunization with HIV Env trimers in rhesus macaques (16). Furthermore, for difficult-to-neutralize pathogens such as HIV, increasing the number of clones entering the GC increases the likelihood that a rare germline B cell targeting a neutralizing epitope could be selected and undergo affinity maturation (8, 17).

One effective approach to enhance the GC response is via the use of extended prime dosing regimens for vaccine administration (18-21). In this approach, a given dose of antigen and adjuvant are provided over a prolonged window of time compared with a traditional bolus vaccine injection, through methods such as repeated injections (18, 19, 21), implanted drug delivery devices (18, 19), or use of slow-release biomaterials (22-24). Among these approaches, a simple strategy that elicits profound changes to humoral immunity is escalating-dose immunization (EDI), where a given dose of vaccine is administered as a series of repeated injections over a period of two weeks. For stabilized HIV Env trimer immunogens, EDI using seven injections in an exponentially-increasing dosing pattern has been shown to increase the magnitude of the GC and Tfh response, increase the number of B cell clones entering the GC, increase the size of the memory B cell response, increase autologous tier 2 neutralizing antibody titers (tier 2 reflecting viruses representative of human isolates rather than lab-adapted strains), and initiate a GC response that can persist for at least 6 months in non-human primates (18, 19, 21, 25).

Although this seven-dose extended-prime regimen is highly effective, it is not practical for mass vaccination (22, 26-28). Our early computational modeling work seeking to understand the mechanisms of EDI immune responses suggested that the key elements driving strong GC responses following EDI are the initiation of B cell priming and GC formation by small amounts of antigen early in the dosing course, followed by later (~one-two weeks) arrival of larger quantities of antigen that can be captured in immune complexes formed via newly-produced affinity-matured antibody in the lymph node (18). This late-arriving antigen is thus captured on FDCs efficiently, providing a reservoir of antigen to drive the GC response. Based on these mechanisms, we hypothesized that a reduced EDI could be possible, simplified to just two injections: a first dose to initiate B cell priming, followed by a second immunization one to two weeks later that would provide antigen for capture on FDCs.

Here, we explored the parameter space of EDI and carried out systematic studies varying the number of doses, dose ratio, and dose intervals using a model HIV Env stabilized trimer immunogen and potent saponin adjuvant in mice. Guided by computational modeling of mechanistic steps required for T cell and B cell priming following bolus or multi-shot immunization, we find that even a two-shot priming approach is able to promote antigen capture by FDCs and retain much of the benefit of the seven-dose EDI regimen in amplifying the humoral response against Env trimers. Together these data suggest that a simple extended-prime immunization approach for subunit vaccines could provide substantial enhancements to humoral immunity.

RESULTS

A two-dose priming regimen augments humoral responses to HIV Env trimer protein immunization over traditional bolus immunization

Using a stabilized HIV Env SOSIP trimer immunogen engineered to promote priming of N332-supersite-directed B cells (N332-GT2 (29)) and a potent saponin nanoparticle adjuvant (saponin/MPLA nanoparticles, SMNP (30, 31)), we conducted an evaluation of varied EDI dosing regimens in mice. Given the large parameter space to explore, we opted

to focus on analysis of GC responses at day 14 for all groups, as we previously found that GCs in mice peaked at this timepoint for immunization patterns as disparate as bolus injection and the full seven-dose ED regimen (18). First, we tested the effect of the number of doses, starting from the previously defined optimal seven-ED regimen, and reducing the number of doses systematically, while keeping the escalation-over-time pattern, the total time interval (12 days), and amount of total vaccine administered (summing all the doses for a given regimen) constant (Fig. 1A). As the number of doses was reduced, the total size of the GC and Tfh responses steadily dropped (Fig. 1B-C). However, staining with fluorescent trimer probes to identify antigen-specific cells, we found the number of trimer-binding GC B cells dropped only ~5-fold moving from seven to three doses, while a two-dose ED pattern was not statistically different from bolus (Fig. 1D, fig. S1A-C). Trimer-specific serum IgG titers measured one month after dosing were similar for seven, six, four, and three-dose ED regimens, but two-dose and bolus immunizations elicited antibody titers eight- and 60-fold lower, respectively (Fig. 1E).

We hypothesized that the poor response to two-dose escalating immunization could be because a 12-day interval between doses is too wide a gap to optimally feed antigen to the GC response. We next tested two-dose patterns administered at intervals ranging from 4 to 12 days, administering 20% of the vaccine dose at day 0, and the remaining 80% at the second injection (Fig. 1F). Here, a two-dose escalating prime immunization with an interval of seven days elicited an optimal response (Fig. 1G-H). Remarkably, this seven-day two-dose pattern elicited 10-fold more trimer-binding GC B cells than bolus immunization, only three-fold fewer than the previously-optimized seven-dose two-week escalating dosing pattern (Fig. 1I).

We next evaluated the impact of the dosing ratio (the proportion of total vaccine administered at dose 1 vs. dose 2, Fig. 1J). Administration of 20% of the vaccine in the first dose was optimal; increasing the initial immunization to 30 or 50% of the total dose led to decaying responses (Fig. 1K-M). This optimized 2-shot regimen administering 20% of the vaccine at day 0 and 80% at day seven (hereafter, 2-ED) induced similar responses as administration of two full vaccine doses a week apart, suggesting that additional antigen at the first dose cannot further augment the GC response (fig. S1D-H). 2-ED priming increased both the size of the GC as well as the proportion of GC B cells recognizing intact antigen, eliciting a six-fold greater frequency of trimer-binding GC B cells compared to bolus vaccination (Fig. 1N). These increased GC responses required that both immunizations were performed at the same site; injection of the second vaccine dose contralaterally led to greatly diminished trimer-binding GC responses in the draining lymph nodes (fig. S1I), suggesting that the second dose is needed to refuel an ongoing GC response in the ipsilateral nodes. Altogether, these data demonstrate that even a minimal two-dose extended priming immunization augments multiple facets of the humoral response to vaccination.

Optimized two-dose ED priming amplifies the magnitude but not the overall lifetime of the GC response

We next assessed the kinetics of humoral responses to the optimized 2-ED regimen compared to bolus immunization (Fig. 2A). Trimer-binding B cells were detectable in both

groups at day seven and peaked at day 14, but total antigen-binding B cells were five-fold greater in the 2-ED group compared to bolus (Fig. 2B). Interestingly, despite the difference in initial vaccine dose administered, GC responses for bolus and 2-dose ED were similar at day seven, but diverged by day 14 (Fig. 2C). GCs in both groups then contracted from day 14 through day 28. The number of Tfh cells in the 2-ED group also sharply expanded between days seven and 14, reaching ~six-fold greater numbers of Tfh cells at the peak of the response at day 14 compared to bolus immunization (Fig. 2D). Trimer-binding GC B cell numbers also peaked for both immunization conditions at day 14, but the 2-ED regimen maintained higher numbers of antigen-specific GC cells through day 21 (Fig. 2E).

Lymph node plasmablasts were expanded by day seven for both the bolus and 2-ED immunizations; these responses peaked at day seven and day 10, respectively, then steadily decayed (Fig. 2F). 2-ED immunizations also impacted the evolution of serum antibody responses. IgM responses primed by bolus immunization peaked at day seven then decayed steadily, while the 2-ED group elicited IgM responses that peaked later, at day 14 (Fig. 2G). Bolus immunization elicited substantial serum IgG titers by day seven, which rose only slightly over the subsequent three weeks (Fig. 2F). By contrast, IgG responses for the 2-ED regimen increased sharply between day seven and 14, reaching titers ~10-fold greater than the bolus group by day 14 that were sustained (Fig. 2H). Hence, the simplified 2-dose ED regimen elicited changes in the humoral response that persisted over many weeks and primed strong, stable serum antibody responses that were greatly increased compared to traditional bolus immunization.

Extended-prime dosing regimens boost innate inflammation in lymph nodes and promote Tfh responses

A strong correlation between the number of Tfh and GC B cells has been observed in prior studies (32, 33), consistent with selection by Tfh cells serving as a key bottleneck controlling proliferation of GC B cells (12, 13, 34, 35). We hypothesized that altered kinetics of antigen and adjuvant availability during ED immunization could substantially impact priming of Tfh cells. To test this idea, we developed a coarse-grained kinetic computational model of the innate immune response and T cell priming following vaccine administration (Fig. 3A, fig. S2A). In this simple model, both antigen (Ag) and adjuvant (Adj) appear as a bolus at an initial administered concentration and clear from the tissue at a constant rate. The adjuvant activates tissue cells at the immunization site and/or draining lymph node (Fig. 3A, (i)), which release cytokines and chemokines that recruit dendritic cells (DCs, Fig. 3A, (ii)). Adjuvant also plays an important role in activating DCs and promoting antigen uptake by these cells (36). As a proxy for these effects, we assume that the adjuvant increases the rate of antigen uptake by DCs and induces DC activation in an Adj and Ag concentration-dependent manner (Fig. 3A, (iii)). Activated, antigen-loaded DCs (aDC^{Ag+}s) then prime T cells in the draining lymph node (Fig. 3A, (iv)). The proliferation of T cells induced by the aDC^{Ag+}s is described according to a previously reported model (37), and we assume proliferating T cells differentiate into Tfh cells at a constant rate (Fig. 3A, (v)). This minimal model is easily interpretable and has a small number of parameters, most of which can be estimated from previous experimental studies (See Supplementary Materials and Table S2 for details on the model and parameter estimation) (38).

We first examined predictions of the number of total DCs, aDC^{Ag+}s, T cells, and Tfh cells following bolus, 2-ED, and 7-ED immunization schemes. After bolus immunization, both total DCs and aDC^{Ag+}s reach their peak within ~one day and then decline due to rapid adjuvant and antigen clearance (Fig. 3B-C). In contrast, the 7-ED regimen shows DCs being periodically recruited with each dose, leading to accumulation in lymph nodes from day ~7 onward (Fig. 3B). The number of aDC^{Ag+}s also gradually increases, reaching a large peak value after day 12 (Fig. 3C). Given the exponential nature of T cell proliferation, extended stimulation by the increasing numbers of aDC^{Ag+}s over time during the 7-ED regimen contributes to the substantially greater peak T cell and Tfh cell counts compared to the bolus (Fig. 3D-E), consistent with previous studies (37, 39). Further, unlike bolus immunization, where antigen decays before most DCs are recruited, a substantial number of DCs are already present in the lymph node at the later 7-ED doses, prominently increasing the number of aDC^{Ag+}s (Fig. 3B-C). For the 2-ED regimen, the model predicts T cells proliferate after the 1^{st} dose, and remain at elevated numbers at the time of the second dose (Fig. 3D). This expanded pool of antigen-specific T cells will then continue to expand on stimulation with the second dose of vaccine. However, with realistic biological parameters, this simple model predicts that DC numbers elevated after the first dose returns to baseline before the second dose (Fig. 3B).

We next modeled each of the escalating-dose regimens tested in Fig. 1C, and found that the model indeed captured the pattern of Tfh responses observed experimentally (Fig. 3F). Note that two parameters in the model, those corresponding to the rate of DC recruitment and the baseline number of T cells, were fitted directly to the experimental data in Fig. 3F (See Supplementary Material for discussion on these parameters). Because of the relationship between adjuvant and DC recruitment/activation, the model also predicts that optimal ED immunization requires co-administration of antigen and adjuvant across the time course. If antigen is administered in an escalating-dose pattern but adjuvant is administered as a bolus, poor synchronization of DC recruitment and antigen availability is predicted, and thus weak Tfh priming (fig. S2B-C). In agreement with this prediction, vaccination of mice with a bolus adjuvant/7-ED antigen dosing schedule elicited much weaker GC and Tfh responses than escalating dosing of antigen and adjuvant together (fig. S2D-E). Thus, this very simple model captures the relative magnitudes of increased Tfh expansion observed for the two different ED regimens compared with traditional bolus immunization.

To test the predictions of the kinetic model, we immunized mice with fluorescently-labeled N332-GT2 trimer and SMNP adjuvant, using ED and bolus dosing schemes. We then analyzed DCs in the draining lymph nodes (dLNs) at key time points post immunization (Fig. 3G, fig. S3). After bolus immunization, both the total number of DCs and activated ($CD86^+$) $trimer^+$ DCs in dLNs increased over 2 days (Fig. 3H-J). The initial dose of 2-ED similarly expanded DCs and activated antigen-loaded DCs over the first two days, though reaching lower peak numbers. DC numbers in the dLNs returned to baseline by day seven, before the second dose was administered, as predicted by the model (Fig. 3H, J). Intriguingly, following the second dose in the 2-ED regimen, the kinetics of DC influx were accelerated compared to the response after the first dose, with a significant increase in activated, antigen-loaded DCs observed as early as 24h post injection (Fig. 3I, J). We hypothesize that the faster kinetics of DC recruitment could be a consequence of

increased antigen presentation and residual inflammation in the dLN from the first dose. In the 7-ED regimen, the accumulation of trimer^{+}CD86^{+} DCs in the lymph nodes becomes markedly evident around day 12. The buildup of DCs peaked following the last dose of the 7-ED regimen on day 12, with peak trimer^{+}CD86^{+} DCs on day 13 more than double those observed with the bolus immunization, in line with model predictions (Fig. 3I-J, also compare Figs. 3J and 3C). We note that while the accumulation of antigen-loaded DCs is not substantially measurable before day 12, even a small number of antigen-loaded DCs may initiate T cell proliferation from the baseline, as suggested by the model (Fig. 3C-D). Given the exponential nature of T cell proliferation, such early proliferation can have considerable importance.

Computational modeling of the GC response predicts improved native antigen capture following extended-prime immunizations

Using a computational model of the GC reaction, we previously predicted that ED immunization can increase the size of the GC response via capture of antigen on follicular dendritic cells (FDCs) (18). However, in the present studies we found that ED dosing also dramatically enhances the proportion of GC B cells that bind to the intact immunogen (10-fold and 6-fold vs. bolus for 7-dose ED and 2-dose ED, respectively, Fig. 1N) (18). In other work, we recently showed that extracellular protease activity in lymph nodes can play an important role in modifying B cell responses, as extracellular antigen accumulated in lymph nodes following bolus vaccination undergoes rapid proteolytic degradation over a period of a few days (40). However, protease activity was found to be low in B cell follicles, such that antigen captured by FDCs could remain intact over prolonged periods (40). To determine if greater amounts of intact antigen captured in follicles could explain the greatly increased proportion of trimer-specific GC B cells detected for ED immunization, we modified our computational model of the B cell and antibody response (35), which combines the cellular dynamics of B cell proliferation and GC B affinity maturation with the kinetics of antibody production and antigen capture, to incorporate effects of antigen degradation (see Supplemental Methods and Table S3 for details on the model and parameter estimation). Briefly, we assume that B cells can target either native antigen or non-native partially degraded antigen, as schematically shown in Fig. 4A. Both types of antigen can be transported to FDCs by the corresponding antibodies that bind to them, where they are protected from further degradation. Additionally, to model the antibody response to HIV Env immunogens, we assume that the non-native antigen is more immunodominant, as HIV Env trimers are heavily glycosylated and present few sites for high affinity antibody binding in the intact state, but are expected to expose more proteinaceous surfaces as they degrade (8).

This revised GC model shows that very small overall amounts of antigen are captured by FDCs following bolus immunization because most of the antigen decays before antigen-specific antibody responses are induced, and very low amounts of immune complexes (IC) are formed (Fig. 4B-D). As a result, highly stringent conditions are maintained for GC B cell survival, resulting in a GC response that is dominated by the immunodominant non-native antigen-targeting B cells. With the 2-ED regimen, a weak antibody response against both the native and non-native antigens is generated after the first dose (Fig. 4C). However, upon the

second dose, this modest titer of antibody is predicted to efficiently form ICs with incoming antigen leading to a dramatic increase in the amount of antigen deposited on FDCs (Fig. 4B,D). The increased antigen availability weakens the immunodominance hierarchy between the two antigens by allowing initially low-affinity B cells to become activated, proliferate and increase affinities through mutations (35). On top of the greater total GC B cell number resulting from improved Tfh cell response (Fig. 4E), this change leads to a much greater fraction of those GC B cells binding to native antigen post-second-dose (Fig. 4F-G). Finally, with 7-ED dosing, the antibody titer is already high when the final dose (63% of vaccine dose) is administered on day 12 (Fig. 4C). Immune complex formation as native antigen arrives at the lymph node at the end of the 7-ED dosing leads to rapid transport of intact immunogen to follicles. This causes the ratio of native vs. non-native antigen presented on FDC to be modestly shifted in favor of the former (Fig. 4D), allowing even better native antigen-binding responses compared to the 2-dose scheme (Fig. 4E-G). Note that native antigen-binding antibody titers at the time of the final dose for 7-ED (on day 12) is greater than that for 2-ED at the time of the final dose (on day 7) (Fig. 4C). These predictions of the GC model align well with the experimentally-measured frequencies of intact trimer-binding GC B cells at day 14 (compare Fig. 4G and Fig. 1N).

A two-dose escalating prime increases antigen capture in follicles compared to bolus immunization

A key prediction of the GC computational model is that a sufficient quantity of antibody specific for intact antigen can be produced by day seven to enable substantial antigen capture on FDCs using the two-dose escalating prime immunization. As shown in Fig. 2G-H, antigen-specific IgM and IgG were both detectable in serum by day seven in the 2-ED regimen. To test the model prediction, we immunized mice with fluorescently-labeled N332-GT2 HIV Env trimer by each of the three dosing schedules, and analyzed the biodistribution of antigen in draining lymph nodes via confocal imaging of histological sections and cleared whole lymph node tissues. As seen in prior studies (18, 19), both cleared whole dLNs (Fig. 5A, fig. S4A-C) and traditional thin section imaging (Fig. 5B, fig. S4D) revealed the presence of substantial amounts of antigen co-localized with FDCs two days following the last dose of the full 7-ED regimen, while little if any antigen could be detected at any location within dLNs 2 days after bolus vaccination. Strikingly, substantial amounts of FDC-localized antigen were also found in draining lymph nodes two days following the second dose of the 2-dose ED immunization (Fig. 5A-B, fig. S4). High magnification imaging of the follicles of the ED groups suggested this follicle-localized antigen was associated with FDC dendrites (Fig. 5B). Flow cytometry analysis of FDCs recovered from pooled LNs of multiple mice immunized with the different dosing regimens revealed that 2-ED or 7-ED immunizations increased the amount of FDC-trapped antigen by 20-fold and 60-fold over bolus immunization, respectively (Fig. 5C-E, fig. S5). Thus, consistent with the computational model of GC dynamics, even a two-dose escalating prime vaccination is capable of achieving antigen targeting to FDCs and greatly increasing the quantity of antigen retained within the LN.

Antibodies mediate antigen trafficking to FDCs by forming immune complexes (ICs) with the antigen and triggering complement deposition on the antigen. Complement-decorated

ICs bind to noncognate B cells, which in turn transfer the ICs to FDCs in a complement- and complement receptor-dependent manner (41-43). Thus, to provide further evidence that early antibody responses are responsible for antigen capture on FDCs in the 2-ED regimen, we compared antigen localization to FDCs following 2-ED vaccination in wild type vs. complement-deficient (C3 knockout) mice. As shown in Fig. 5F-G, antigen capture in the lymph node was greatly reduced in C3 knockout animals, suggesting that the early antibody response is important for antigen delivery to FDCs in this dosing regimen.

A second potential factor that could promote antigen capture following 2-ED dosing is the disruption of sinus-lining macrophages by the initial dose of the SMNP adjuvant: We previously found that SMNP induces rapid elimination of subcapsular sinus macrophages within ~24 hours following dosing, and are not replenished until ~14 days later; this deletion of macrophages was associated with enhanced antigen entry into lymph nodes (30). We thus tested whether the low dose of SMNP used in the first injection of the 2-ED regimen (1 μg per mouse) was capable of similarly leading to loss of sinus macrophages. Enumeration of lymph node cells by flow cytometry 24 hr after dosing revealed that this low dose of SMNP indeed eliminated subcapsular sinus macrophages as efficiently as our standard adjuvant dosing (fig. S4E). This may provide a second mechanism promoting antigen accumulation on FDCs during the 2-ED vaccination regimen.

Extending antigen availability on the second immunization further boosts humoral responses as a consequence of enhanced native antigen presentation

Given that the computational model of the GC reaction is able to provide qualitatively accurate predictions of the observed GC size and proportion of antigen-specific GC B cells, we next used the model to explore a much wider parameter space of dosing patterns than would be possible experimentally, to gain further insight into how humoral responses might be further bolstered using extended priming. The modeling and experimental data suggest that having a high trimer-binding antibody titer present before the majority of the antigen dose is administered is an important factor governing the magnitude of the “on target” GC response. In the 2-ED prime immunization, antibody titers increase steadily after the 2nd injection (Fig. 2H and Fig. 4C). However, because intact antigen in the lymph node decays rapidly (estimated half-life ~6.2 hours, Table S1), most of the antigen arriving after the second immunization decays before high titers of antibody are reached, leading to presentation of a substantial amount of non-native antigen on FDCs. Thus, we hypothesized that extending antigen availability over a longer time period at the second dose might further substantially enhance trimer-binding GC responses. We simulated a 2-dose ED regimen where antigen was released from the injection site at a constant rate over 10 days after the second injection (Fig. 6A). In this case, much of the antigen dose arrives at the dLN after high titers of trimer-specific antibody are generated and is thus captured in immune complexes in an intact state (Fig. 6B-C). Compared to 2-ED dosing using bolus injections, the fraction of intact antigen among ICs increases from ~38% to 92% with the slow-release second dose (Fig. 6D). The model predicts that this in turn leads to a superior trimer-specific GC B cell response compared to the 2-dose immunization (Fig. 6E-F). Varying the duration of antigen delivery after the second dose shows that a longer release duration leads to higher

fraction of native antigen on FDCs (Fig. 6G) and better trimer-specific GC B cell response (Fig. 6H-I), highlighting the importance of dosing kinetics.

To experimentally test this idea, we employed an approach we previously developed (27) to achieve slow-delivery effects in a manner readily translatable to clinical use: a stabilized HIV Env trimer termed MD39 (44) (very similar in sequence to the N332-GT2 trimer) was conjugated with short phosphoserine (pSer) peptide affinity tags (one tag per protomer at the C-termini located at the base of the trimer). Phosphate groups in the affinity tags undergo a ligand exchange reaction with the surface of alum particles, enabling oriented high-avidity binding of the trimer to aluminum hydroxide adjuvant (Fig. 6J). By stably anchoring the antigen to alum particles, the antigen is slowly released from the injection site as alum particles slowly disaggregate over time (27, 31, 45). Using this simple approach, alum-adsorbed MD39 trimers that normally clear from the injection site within a few days instead clear much more slowly, over ~10 days (27). We thus tested a two-dose ED immunization giving 20% of the vaccine dose on day 0 as a bolus and 80% of the dose as an alum/pSer-trimer formulation on day seven. Total GC B cells and Tfh cells elicited were similar between the 2-ED and 2-ED (alum-pSer) groups (Fig. 6K-L). However, relative to the bolus 2-ED immunization, extended antigen delivery provided by alum particle anchoring of the second shot in the 2-ED (alum-pSer) group trended towards improved responses, eliciting a 2.5-fold increase in the frequency of intact trimer-binding GC B cells and a 2-fold increase in the absolute number of these trimer-specific cells (Fig. 6M-O). These observations are consistent with model predictions (Fig. 6E-F). Interestingly, using the pSer-alum anchoring approach for both shots of the 2-dose regimen showed no improvement in trimer-specific GC responses over using it only for the 2nd shot (fig. S6A-C) indicating that the benefit of constant release of antigen is more relevant once high antibody titers are present to enable capture of the native antigen. *In silico* simulation of this scenario agrees with this experimental observation (fig. S6D-E). Thus, an engineered 2-dose immunization, providing an initial “priming” dose followed by a larger extended-release vaccine dose retains much of the benefit to the GC response and fully amplifies the serum antibody response, substantially greater than bolus immunization.

DISCUSSION

In previous studies, we discovered that prolonging vaccine availability through extended dosing strategies enhances multiple facets of the immune response (16, 18, 19). In particular, an escalating-dose immunization of 7 shots administered in an exponentially-increasing dose pattern over two weeks was particularly effective in both mice and non-human primates for promoting humoral responses to HIV Env immunogens (18, 19, 21, 25). However, administering seven doses is not practical for mass vaccination. Through systematic studies varying the number of doses, dose ratio, and dose intervals in mice, we found that a two-shot reduced ED regimen, administering 20% of the vaccine dose on day 0 and 80% on day 7, elicited 5-10-fold increases in peak antigen-binding total B cells (Fig. 2B) and GC B cells (Fig. 1N, 2E), respectively, and increased serum antibody responses 60-fold relative to bolus immunization (Fig. 2H). Such a scenario- two shots administered 1-2 weeks apart, would not be out of the realm of practicality (e.g., compare to current COVID-19 mRNA vaccines, administered twice at a 3- or 4-week interval). Clinically, the two-dose regimen developed

here might most easily be implemented by administering two full doses of vaccine at the proper interval, rather than preparing different doses for the first vs. second shot. As shown in fig. S1, this dosing also greatly amplifies the GC response. However, short-interval "full" dosing might promote undesirable reactogenicity, depending on the adjuvant employed. Such a dosing scheme should not be conflated with a traditional prime-boost approach, where a second dose is given 3 weeks to several months after the priming immunization. In the latter traditional dosing scenario, B cells are being recalled and may or may not be interacting with GCs induced by the priming immunization, whereas in the 2-ED regimen, vaccine administered in the second shot is meant to augment the ongoing GC initiated by the first injection.

By combining computational modeling and experimental studies, we found that 2-ED priming promotes substantial antigen capture on FDCs, compared to very limited antigen capture following bolus immunization. However, this is not the only effect of the extended-prime dosing. 2-ED immunization also increased Tfh responses (by 6-fold over bolus at the peak of the response, Fig. 2D). Tfh cells are essential for the GC reaction, providing support to B cells to generate long-lived plasma cells and memory B cells (46-48). The development of Tfh cells is initiated by priming of naïve T cells by DCs (48). The 2-shot immunization leads to a rapid increase in MHC-II^{+} DCs after the 2nd dose, which may continue the expansion of T cells initially primed after the first dose (49, 50). This mechanistic insight highlights the strong influence of temporal dosing dynamics on Tfh cell priming. In comparison, although immunization with nanoparticle antigens have been shown to also achieve antigen deposition on FDCs, studies have reported mixed results on whether they improve Tfh responses (51). In our computational model of the germinal center response, we find that an enhanced priming of the Tfh response from an escalating-dose regimen promotes both entry of B cells into GCs and their positive selection in GCs, leading to increased GC B cell numbers (Fig. 4E). However, this enhanced Tfh response can support entry and selection of both antigen-specific and non-native epitope-binding GC B cells. This can occur because internal peptides that comprise T cell epitopes are less affected by antigen degradation (51). But extended dosing also promotes the deposition of intact antigen on FDCs. This gives antigen-specific GC B cells a competitive advantage over those that bind to non-native epitopes when interacting with Tfh cells (Fig. 4G) (52, 53).

Our findings have broad implications for designing vaccine dosing regimens. With extended dosing, availability of intact antigen in the lymph node is synchronized with the developing GC response. We observed that for the 7-ED regimen, amplification of GC and Tfh cells occurs towards the end of the dosing schedule, corresponding to the timing when antigen capture on FDCs is most prominent. The computational model suggests that an important mechanism underlying the efficacy of extended dosing regimens is the improved capture of native antigen on FDCs. In a simplified 2-shot immunization, administering a majority of the antigen on the 2nd shot allows for exploitation of pre-existing antibody responses induced by the lower 1st dose, maximizing the quantity of the immunogen dose captured in immune complexes. The computational model further predicts that if antigen is slowly released at the 2nd dose, increased representation of antigen in native form on FDCs can further promote intact antigen-specific GC responses. This is in contrast to bolus immunization where only a small amount of antigen is presented on FDC to GC B cells, much of which is non-native

protein and breakdown products that can be immunodominant and distract the GC response from relevant targets (54, 55). These predictions were positively tested by our experiments. More antigen on FDCs during later stages of a GC likely increases GC B cell clonotypic diversity, allowing for more BCR sequence space to be explored for high affinity BCR mutations.

A limitation of this study is that immune response dynamics, and particularly the kinetics of the GC response, may differ in mice vs. non-human primates or humans. We expect the key elements of this strategy to be valid across species, but the ideal dosing ratio and dosing interval for a 2-ED regimen in NHPs or humans will require experimental evaluation. Our computational model also neglects some features of GC reactions. However, we have shown that mechanistic insights emerging from similar computational models have been tested positively by experiments and clinical data, as in this study. Priming immunization through 2 injections is also still less ideal than vaccination at a single timepoint. However, several technologies are being developed to recapitulate the effects of ED dosing following a single injection, For example, biodegradable polymer formulations have been demonstrated that achieve programmed timing of vaccine release at the injection site (56), and slow-dissolving alum coatings have been developed that may enable vaccine to be released over tunable time periods *in vivo* (28). Our findings provide a strong rationale for continued development of these approaches.

MATERIALS & METHODS

Study design

The primary aim of this research was to assess the impact of extended prime immunizations on humoral responses to subunit vaccine immunization, compared to traditional bolus immunization in mouse models. To achieve this goal, we immunized mice with clinically relevant subunit protein immunogens in combination with saponin adjuvants, and evaluated early (antigen uptake and induction of Tfh and GC) and late (lymph node and serum antibody) responses over time. Mechanistic studies were conducted to examine antigen acquisition and activation of antigen-specific B and T cells, as well as computational analyses of the germinal center response to parse out differences in the dosing regimens. For animal experiments, the investigators were not blinded to the group identities.

Immunogens

N332-GT2 trimers were expressed in FreeStyle 293F cells (Invitrogen, Cat no. R79007) and purified in two steps by affinity chromatography using a GE HisTrap column and size-exclusion chromatography using a GE S200 Increase column as described previously (29, 57). MD39 HIV Env trimer with free C-terminal cysteines was generated as previously described (57). Both trimers were administered at a dose of 10 ug per animal.

pSer-conjugation

MD39 trimer immunogens bearing a free C-terminal cysteine at a concentration of 1 mg/ml were reduced by incubation with 10 molar equivalents of tris(2-carboxyethyl)phosphine (TCEP, ThermoFisher), followed by incubation at 25°C for 10 minutes. The reduced protein

solutions were then processed using Amicon Ultra Centrifugal Filters (10 kDa MWCO, Millipore Sigma) to remove TCEP, and the resulting protein was mixed with 5 molar equivalents of pSer-maleimide linkers at a concentration of 1 mg/ml for 16 hours at 4°C in tris-buffered saline (TBS, Sigma Aldrich) at pH 7.2-7.4. After the reaction, unreacted pSer linker was removed using centrifugal filters in TBS, and pSer-antigen was buffer exchanged to PBS.

Adjuvant preparation

The saponin adjuvant used in this study, SMNP, is an ISCOM-like self-assembled nanoparticle consisting of Quillaja saponin, cholesterol, DPPC, and MPLA (30). Briefly, solutions of cholesterol (20mg/ml final concentration, Avanti Polar Lipids Cat# 700000), DPPC (20mg/ml final concentration, Avanti Polar Lipids Cat# 850355), and MPLA (10mg/ml final concentration, PHAD) were prepared in Milli-Q water containing 20% w/vol MEGA-10 (Sigma D6277) detergent. Quil-A saponin (InvivoGen vac-quil) was dissolved in Milli-Q water at a final concentration of 100 mg/ml. All components were mixed at a molar ratio of 10:10:2.5:1 (Quil-A:chol:DPPC:MPLA) followed by dilution with PBS to a final concentration of 1 mg/ml cholesterol. The solution was allowed to equilibrate overnight at room temperature, followed by dialysis against PBS using a 10k MWCO membrane. The adjuvant solution was then sterile filtered, concentrated using 50k MWCO centricon spin filters, and further purified by FPLC using a Sephacryl S-500 HR size exclusion column. Doses are reported in terms of the amount of saponin administered, calculated by measuring the concentration of cholesterol (Cholesterol Quantitation kit; Millipore Sigma; Cat# MAK043) in the preparation and assuming quantitative incorporation of the saponin during synthesis.

Antigen labeling and characterization

A 1 mg/mL solution of protein antigen (N332-GT2) in PBS was mixed with an equal volume of 0.2 M sodium bicarbonate buffer (pH 8.4) on ice. A fresh stock solution of Sulfo-Cyanine 5 NHS ester was prepared at a concentration of 1 mg/mL in 0.2 M sodium bicarbonate buffer (pH 8.4) and added to the antigen solution. The mixture was incubated at 4°C for 16 hours, and then desalted twice using a Zeba Spin Desalting column equilibrated in PBS. The labeled antigen was filtered through 0.22 μm pore size Spin-X centrifuge tube filters and stored at 4°C until use. The degree of labeling of the antigen was determined by measuring the absorbance at 280 and 646 nm wavelengths for total protein and Cy5 dye, respectively. Extinction coefficient values of 113215 and 271000 $M^{-1}cm^{-1}$ were used to calculate the relative concentrations of one subunit of N332-GT2 Trimer and sulfo-cy5 NHS ester, respectively. The degree of labeling for soluble antigen was determined by calculating the ratio of antigen concentration to Cy5 concentration.

Mice

All mouse studies were performed under a protocol approved by the Institutional Animal Care and Use Committee (IACUC) at MIT following all local and federal guidelines for humane animal use. Studies were performed using 8-week-old female C57BL/6J mice (Strain 000664, Jackson Laboratory) and B6.129S4-*C3*^{tm1Crr}/J mice (Strain 029661, Jackson Laboratory). Experiments were performed in specific pathogen-free animal facilities at the

MIT Koch Institute for Integrative Cancer Research. Mice were housed under standard 12-hour light-12-hour dark conditions with ad libitum access to water and chow.

Immunizations and sample collections

8-week-old female C57BL/6 mice were anesthetized and immunized with 10 μg of indicated antigens in the presence of 5 μg saponin adjuvant (SMNP) subcutaneously, with half of the dose administered on each side of the tail base. In the case of the pSer-conjugated MD39 trimer antigen, immunizations were prepared by mixing 10 μg of antigen and 50 μg of alum in 100 μl of sterile TBS (Sigma-Aldrich Alhydrogel, catalog no. T5912) per mouse unless otherwise specified. Antigen was loaded onto alum for 30 min on a tube rotator after which 5 μg of SMNP was added into the immunization and incubated with antigen-alum formulations for 30 min before immunization. Blood (from submandibular; 100 μL) was collected at indicated time-points into serum separator tubes (BD Corporation) and centrifuged at 4,000 × g for 10 min at 4 °C. Sera extracted from blood samples were stored at −80 °C until ready for analysis. Inguinal LNs were harvested and added to Eppendorf tubes containing Protease inhibitor buffer (containing protease inhibitor cocktail and EDTA in PBS with 2% FBS). LNs were processed using a pestle and centrifuged at 16,000g for 5 min at 4 °C to pellet the cell/tissue debris. Supernatant was transferred to Spin-X tubes (Corning™ Costar™) and centrifuged again for 5 min with the flow through being transferred to final collection tubes, flash frozen and stored at −80 °C until ready for analysis.

ELISA

High-binding ELISA plates (07-200-37, Fisher Scientific) were coated with 1 mg/ml trimer and blocked with 2% BSA in PBS overnight. To detect antigen-specific IgG responses, dilutions of serum or lymph node aspirate were added to the wells and incubated for 1.5 hours at 25°C. Plates were washed three times in PBS containing 0.2% Tween-20, and then anti-mouse IgG secondary antibody conjugated to HRP (172-1011, Bio-Rad Laboratories), diluted 1:5000 in blocking buffer as per manufacturer instructions, was added to the wells. After 1 hour of incubation, plates were washed, developed with TMB, and the reaction was stopped with sulfuric acid. The optical density of the mixture was read out at 450 nm subtracting the absorbance at 540 nm according to the manufacturer's instructions.

Immunofluorescence staining

Inguinal lymph nodes (LNs) extracted from euthanized mice were submerged into cryomolds containing O.C.T. (23-730-571, Fisher Scientific) compound and dipped into 2-methylbutane (M32631, Millipore Sigma) pre-chilled in liquid nitrogen. All frozen tissues were cryosectioned on a Leica CM1950 at 10 μm thickness, adhered to Superfrost Plus microscope slides (12-550-15, Fisher Scientific), and stored in −80°C until use. Frozen sections were retrieved from −80°C, quickly thawed, and incubated in 4% paraformaldehyde for 10 minutes at 25°C. The sections were washed 3 times in PBS with 10-minute incubation time between each wash. Excess PBS was removed after the final wash before incubating the slides in blocking buffer, comprised of 2% BSA and 2% Triton X-100 in PBS. After 30 minutes, the blocking buffer was aspirated and the slides were stained in 1:75 anti-CD35 (740029, BD Biosciences) primary antibody solution also made in blocking buffer for ~16

hours at 4°C. These slides were washed in PBS 3 times for 10 min, stained with 1:200 diluted secondary antibodies solution in blocking buffer (ab150063 Abcam, ab150061, Abcam) for 4 hours at room temperature, and washed again in PBS. To mount the slides, one drop of ProLong Diamond Antifade Mountant (Thermo) was added directly onto the stained tissues prior to gently placing a 20x20 mm coverslip on top of the droplet to sandwich the section. The coverslip was sealed using CoverGrip coverslip sealant (23005, Biotium) and imaged immediately. For all experiments, imaging was performed on a Leica SP8 confocal microscope equipped with a white light laser and spectral emission filter to detect emission wavelengths between 470 and 670 nm with a minimum bandwidth of 10 nm. All images were recorded with a 25X water immersion lens and a 63X oil immersion lens for assessing antigen drainage in the LNs, laser settings were kept constant across different time points for each immunogen.

Whole tissue imaging

For whole tissue imaging, mice were injected subcutaneously with anti-CD35 BV421 antibody (clone 8C12, 4 μg per mouse) and lymph nodes were isolated 16 hours later and fixed overnight in 4% paraformaldehyde. Tissues were then processed with a modified DISCO protocol as previously described (58). Briefly, the nodes were washed twice in PBS and excess fat and connective tissue was removed, then placed in solutions containing successively higher concentrations (20, 50, 80%, 100%) of methanol for 30 mins each. Tissues were then bleached for 2 minutes in hydrogen peroxide, returned to methanol for 30 min, then incubated in solutions containing increasing concentrations of tertiary-butanol (20, 50, 80%, 100%) for one hour each at 37° C. All solutions used after bleaching contained an additional 0.4% α-tocopherol (vitamin E). Nodes were then removed from solution and allowed to dry completely before being placed in dichloromethane for delipidation. After the lymph nodes dropped to the bottom of tubes following swirling (indicating removal of remaining tertiary-butanol), they were stored in dibenzyl ether with 0.4% α-tocopherol, which was used as a refractive index matching solution. Cleared lymph nodes were imaged using an Olympus FV1200 Laser Scanning Confocal Microscope at 10x magnification. Lasers were set to minimize pixel saturation in the brightest samples. All laser and channel settings were then kept constant across groups for direct comparison between different samples. Each lymph node was imaged over a depth of 300 μm with line average of 3. Colocalization of N332 and ant-CD35 signal was determined by Pearson's correlation through ImageJ analysis of 100-300 micron z-stacks of immunized LNs. FDC occupancy calculations were performed with a MATLAB script, where images for each channel were smoothed with a 3-D Gaussian filter (sigma = 0.5), then binarized into a mask to identify follicle or antigen area. The fraction of FDC area occupied by antigen was achieved by calculating overlapping pixels in the two binary masks. This calculation was performed for each individual image in the z-stack (9 per image), as well as for the z-projection (sum of slices).

Flow Cytometry Analysis of Lymph Nodes

Inguinal lymph nodes were harvested and single-cell suspensions were obtained by crushing tissues through a 70-μm filter (BD Biosciences). Isolated cells were stained with Live/Dead fixable aqua stain (L34957, Thermo Fisher Scientific) for 10 min at 25°C before

washing twice in flow cytometry buffer (PBS containing 2% fetal bovine serum and 2 mM ethylenediaminetetraacetic acid, EDTA). Cells were then incubated with Fc block (101319, BioLegend) for 10 min at 4°C before staining with antibodies listed (see Supplementary Table S4) for 30 additional min at 4°C. For trimer-specific GC B cell analysis, cells stained with antibodies were distributed evenly and exposed at a 1:100 dilution in 50ul of flow cytometry buffer to biotinylated trimer preincubated with streptavidin (30 min at molar ratio of 1:4 at 25°C) conjugated to phycoerythrin (405203, BioLegend) or BV421 (405226, BioLegend) for 30 minutes at 4°C. Flow cytometry was carried out on a BD LSR Fortessa or LSR II. To assess GC B cells, cells were stained with GL7 PerCPCy5.5 (GL7; BioLegend), CD38 FITC (90; BioLegend), B220 PE-Cy7 (RA3-6B2; BioLegend), and CD4 BV711 (GK1.5; BioLegend). To assess Tfh cells, cells were stained with CD4 BV711 (GK1.5; BioLegend), B220 PE-Cy7 (RA3-6B2; BioLegend), CXCR5 PE (phycoerythrin) (L138D7; BioLegend), and PD1 BV421 (29F.1A12; BioLegend). Dead cells were stained using Fixable Aqua Dead Cell Stain kit (Thermo Fisher Scientific).

FDC Analysis via Flow Cytometry

For each pooled sample, 4 draining inguinal LNs from 2 mice were harvested after euthanasia and maintained in 40 μL of chilled PBS within 1.5 mL Biomasher Tubes. Digestion buffer was subsequently prepared by dissolving of 0.4 U/mL Dispase (Stemcell Technologies), 0.1 mg/mL Collagenase D, and 0.1 mg/mL DNAse in RPMI-1640. For each pooled sample, 1 mL of digestion buffer was added into the Biomasher tubes and the LNs within were mechanically dissociated. The tissue mixture was then placed into an end-to-end rotator and incubated at 37° C for 20 minutes. Thereafter, the mixture was allowed to sediment for 1 minute and ~900 μL of the supernatant was transferred into 10 mL of flow cytometry buffer containing 1% BSA and 5 mM EDTA dissolved in PBS to stop the digestion. The digestion and neutralization process was repeated once more. The flow cytometry buffer containing the liberated cells was centrifuged at 500x*g* for 5 minutes prior to discarding the supernatant and resuspending in 250 μL of flow cytometry buffer. This solution was passed through a 70 μm filter mesh and processed in 96 well V-bottom plates for flow cytometry. All liberated cells were stained with Live/Dead fixable aqua stain (L34957, Thermo Fisher Scientific), anti-CD45 (BUV395, Clone: 30-F11), anti-GP38 (Biotin, Clone: 8.1.1), anti-CD31 (PE, Clone: 390), anti-CD35 (BV421, Clone: 8C12), and anti-EpCAM (BV785, Clone: G8.8) antibodies before analysis with BD Symphony A3. Care was taken to analyze nearly all of the isolated cells and at lowest flow rates to ensure maximal number of stromal cells are recorded. FDCs were identified as $CD45^{-}$, $CD31^{-}$, $GP38^{+}$, $CD35^{+}$, and $EpCAM^{+}$. Antigen-positive FDCs cells were gated based on background Cy5 fluorescence from FDCs isolated from naïve mice.

Statistical analysis

Statistical analysis and graphing were done with GraphPad Prism for the experimental data and with MATLAB Statistics and Machine Learning Toolbox for the simulation data. The two-tailed Student's *t* test was used to compare two experimental groups and one-way Anova with Dunnett's multiple comparison post hoc analysis was used for comparing more than two groups. Details of the statistical test and number of replicates are indicated in the figure legends. A value of $P<0.05$ was considered statistically significant.

Mathematical model

The coarse-grained model of T cell priming by antigen and adjuvant was formulated by integrating insights from experimental literature (30, 59-64) with a previously published model of T cell proliferation (37). The system of ordinary differential equations is summarized in Fig. S2A, and a detailed description of the model and parameters is provided in Supplementary Materials. The model for the GC B cell response was adapted with minor modifications from a previous published study (35). A comprehensive overview of the model, including the equations, parameters, and the details of the modifications made, is provided in the Supplementary Materials.

Statistical analysis

Statistical analyses and graphing were carried out using GraphPad Prism for the experimental data and with MATLAB Statistics and Machine Learning Toolbox for the simulation data. The two-tailed Student's *t* test was used to compare two experimental groups and one-way Anova with Dunnett's multiple comparison post hoc analysis was used for comparing more than two groups. Details of the statistical test and number of replicates are indicated in the figure legends. A value of $P<0.05$ was considered statistically significant.

Supplementary Material

Refer to Web version on PubMed Central for supplementary material.

Acknowledgements

We thank the Koch Institute's Robert A. Swanson (1969) Biotechnology Center for technical support, specifically the Flow Cytometry and Microscopy Facilities.

Funding:

This work was supported in part by the Koch Institute Core Grant (P30-CA14051) from the National Cancer Institute, the NIH (awards AI161297, AI125068, and UM1AI144462 to D.J.I and AI175489 to D.J.I and A.K.C and F99CA264404 to S.H.B), and the Ragon Institute of MIT, MGH, and Harvard. L.Y was also supported by NIH grant # U19AI057229.

REFERENCES

1. Barouch DH, Covid-19 Vaccines — Immunity, Variants, Boosters. New Engl J Med 387, 1011–1020 (2022). [PubMed: 36044620]
2. Lee JH, Crotty S, HIV vaccinology: 2021 update. Semin Immunol 51, 101470 (2021). [PubMed: 34272086]
3. Haynes BF, Wiehe K, Borrow P, Saunders KO, Korber B, Wagh K, McMichael AJ, Kelsoe G, Hahn BH, Alt F, Shaw GM, Strategies for HIV-1 vaccines that induce broadly neutralizing antibodies. Nat Rev Immunol 23, 142–158 (2023). [PubMed: 35962033]
4. Feinberg MB, Uhambo — Twists and Turns on the Journey to an Efficacious HIV-1 Vaccine. New Engl J Med 384, 1157–1159 (2021). [PubMed: 33761212]
5. Burton DR, Advancing an HIV vaccine; advancing vaccinology. Nat Rev Immunol 19, 77–78 (2019). [PubMed: 30560910]
6. Gilbert PB, Huang Y, deCamp AC, Karuna S, Zhang Y, Magaret CA, Giorgi EE, Korber B, Edlefsen PT, Rossenkhan R, Juraska M, Rudnicki E, Kochar N, Huang Y, Carpp LN, Barouch DH, Mkhize NN, Hermanus T, Kgagudi P, Bekker V, Kaldine H, Mapengo RE, Eaton A, Domin E, West C, Feng

W, Tang H, Seaton KE, Heptinstall J, Brackett C, Chiong K, Tomaras GD, Andrew P, Mayer BT, Reeves DB, Sobieszczyk ME, Garrett N, Sanchez J, Gay C, Makhema J, Williamson C, Mullins JI, Hural J, Cohen MS, Corey L, Montefiori DC, Morris L, Neutralization titer biomarker for antibody-mediated prevention of HIV-1 acquisition. Nat Med 28, 1924–1932 (2022). [PubMed: 35995954]

7. Corey L, Gilbert PB, Juraska M, Montefiori DC, Morris L, Karuna ST, Edupuganti S, Mgodi NM, deCamp AC, Rudnicki E, Huang Y, Gonzales P, Cabello R, Orrell C, Lama JR, Laher F, Lazarus EM, Sanchez J, Frank I, Hinojosa J, Sobieszczyk ME, Marshall KE, Mukwekwerere PG, Makhema J, Baden LR, Mullins JI, Williamson C, Hural J, McElrath MJ, Bentley C, Takuva S, Lorenzo MMG, Burns DN, Espy N, Randhawa AK, Kochar N, Piwowar-Manning E, Donnell DJ, Sista N, Andrew P, Kublin JG, Gray G, Ledgerwood JE, Mascola JR, Cohen MS, H. 704/HPTN 085 and H. 703/HPTN 081 S. Teams, Two Randomized Trials of Neutralizing Antibodies to Prevent HIV-1 Acquisition. New Engl J Med 384, 1003–1014 (2021). [PubMed: 33730454]
8. Havenar-Daughton C, Lee JH, Crotty S, Tfh cells and HIV bnAbs, an immunodominance model of the HIV neutralizing antibody generation problem. Immunol Rev 275, 49–61 (2017). [PubMed: 28133798]
9. Klasse PJ, Ozorowski G, Sanders RW, Moore JP, Env Exceptionalism: Why Are HIV-1 Env Glycoproteins Atypical Immunogens? Cell Host Microbe 27, 507–518 (2020). [PubMed: 32272076]
10. Krammer F, Palese P, Advances in the development of influenza virus vaccines. Nat. Rev. Drug Discov 14, 167–182 (2015). [PubMed: 25722244]
11. Krammer F, Palese P, Universal Influenza Virus Vaccines That Target the Conserved Hemagglutinin Stalk and Conserved Sites in the Head Domain. J. Infect. Dis 219, S62–S67 (2019). [PubMed: 30715353]
12. Victora GD, Nussenzweig MC, Germinal Centers. Annu Rev Immunol 40, 1–30 (2022). [PubMed: 34871102]
13. Victora GD, Nussenzweig MC, Germinal Centers. Immunology 30, 429–457 (2012).
14. Shulman Z, Gitlin AD, Weinstein JS, Lainez B, Esplugues E, Flavell RA, Craft JE, Nussenzweig MC, Dynamic signaling by T follicular helper cells during germinal center B cell selection. Science 345, 1058–1062 (2014). [PubMed: 25170154]
15. Gitlin AD, Mayer CT, Oliveira TY, Shulman Z, Jones MJK, Koren A, Nussenzweig MC, T cell help controls the speed of the cell cycle in germinal center B cells. Science 349, 643–646 (2015). [PubMed: 26184917]
16. Pauthner M, Havenar-Daughton C, Sok D, Nkolola JP, Bastidas R, Boopathy AV, Carnathan DG, Chandrashekar A, Cirelli KM, Cottrell CA, Eroshkin AM, Guenaga J, Kaushik K, Kulp DW, Liu J, McCoy LE, Oom AL, Ozorowski G, Post KW, Sharma SK, Steichen JM, de Taeye SW, Tokatlian T, de la Peña AT, Butera ST, LaBranche CC, Montefiori DC, Silvestri G, Wilson IA, Irvine DJ, Sanders RW, Schief WR, Ward AB, Wyatt RT, Barouch DH, Crotty S, Burton DR, Elicitation of Robust Tier 2 Neutralizing Antibody Responses in Nonhuman Primates by HIV Envelope Trimer Immunization Using Optimized Approaches. Immunity 46, 1073–1088.e6 (2017). [PubMed: 28636956]
17. Abbott RK, Lee JH, Menis S, Skog P, Rossi M, Ota T, Kulp DW, Bhullar D, Kalyuzhniy O, Havenar-Daughton C, Schief WR, Nemazee D, Crotty S, Precursor Frequency and Affinity Determine B Cell Competitive Fitness in Germinal Centers, Tested with Germline-Targeting HIV Vaccine Immunogens. Immunity 48, 133–146.e6 (2018). [PubMed: 29287996]
18. Tam HH, Melo MB, Kang M, Pelet JM, Ruda VM, Foley MH, Hu JK, Kumari S, Crampton J, Baldeon AD, Sanders RW, Moore JP, Crotty S, Langer R, Anderson DG, Chakraborty AK, Irvine DJ, Sustained antigen availability during germinal center initiation enhances antibody responses to vaccination. Proc National Acad Sci 113, E6639–E6648 (2016).
19. Cirelli KM, Carnathan DG, Nogal B, Martin JT, Rodriguez OL, Upadhyay AA, Enemuo CA, Gebru EH, Choe Y, Viviano F, Nakao C, Pauthner MG, Reiss S, Cottrell CA, Smith ML, Bastidas R, Gibson W, Wolabaugh AN, Melo MB, Cossette B, Kumar V, Patel NB, Tokatlian T, Menis S, Kulp DW, Burton DR, Murrell B, Schief WR, Bosinger SE, Ward AB, Watson CT, Silvestri G, Irvine DJ, Crotty S, Slow Delivery Immunization Enhances HIV Neutralizing Antibody and Germinal Center Responses via Modulation of Immunodominance. Cell 177, 1153–1171.e28 (2019). [PubMed: 31080066]

20. Irvine DJ, Aung A, Silva M, Controlling timing and location in vaccines. Adv Drug Deliver Rev, doi: 10.1016/j.addr.2020.06.019 (2020).
21. Lee JH, Sutton HJ, Cottrell CA, Phung I, Ozorowski G, Sewall LM, Nedellec R, Nakao C, Silva M, Richey ST, Torres JL, Lee W-H, Georgeson E, Kubitz M, Hodges S, Mullen T-M, Adachi Y, Cirelli KM, Kaur A, Allers C, Fahlberg M, Grasperge BF, Dufour JP, Schiro F, Aye PP, Kalyuzhniy O, Liguori A, Carnathan DG, Silvestri G, Shen X, Montefiori DC, Veazey RS, Ward AB, Hangartner L, Burton DR, Irvine DJ, Schief WR, Crotty S, Long-primed germinal centres with enduring affinity maturation and clonal migration. Nature 609, 998–1004 (2022). [PubMed: 36131022]
22. Boopathy AV, Mandal A, Kulp DW, Menis S, Bennett NR, Watkins HC, Wang W, Martin JT, Thai NT, He Y, Schief WR, Hammond PT, Irvine DJ, Enhancing humoral immunity via sustained-release implantable microneedle patch vaccination. Proc National Acad Sci 116, 16473–16478 (2019).
23. Roth GA, Gale EC, Alcántara-Hernández M, Luo W, Axpe E, Verma R, Yin Q, Yu AC, Hernandez HL, Maikawa CL, Smith AAA, Davis MM, Pulendran B, Idoyaga J, Appel EA, Injectable Hydrogels for Sustained Codelivery of Subunit Vaccines Enhance Humoral Immunity. Acs Central Sci 6, 1800–1812 (2020).
24. Gale EC, Powell AE, Roth GA, Meany EL, Yan J, Ou BS, Grosskopf AK, Adamska J, Picece VCTM, d'Aquino AI, Pulendran B, Kim PS, Appel EA, Hydrogel-Based Slow Release of a Receptor-Binding Domain Subunit Vaccine Elicits Neutralizing Antibody Responses Against SARS-CoV-2. Adv. Mater 33, 2104362 (2021). [PubMed: 34651342]
25. Steichen JM, Phung I, Salcedo E, Ozorowski G, Willis JR, Baboo S, Liguori A, Cottrell CA, Torres JL, Madden PJ, Ma KM, Sutton HJ, Lee JH, Kalyuzhniy O, Allen JD, Rodriguez OL, Adachi Y, Mullen T-M, Georgeson E, Kubitz M, Burns A, Barman S, Mopuri R, Metz A, Altheide TK, Diedrich JK, Saha S, Shields K, Schultze SE, Smith ML, Schiffner T, Burton DR, Watson CT, Bosinger SE, Crispin M, YatesIII JR, Paulson JC, Ward AB, Sok D, Crotty S, Schief WR, Vaccine priming of rare HIV broadly neutralizing antibody precursors in nonhuman primates. Science 384, eadj8321 (2024). [PubMed: 38753769]
26. Roth GA, Picece VCTM, Ou BS, Luo W, Pulendran B, Appel EA, Designing spatial and temporal control of vaccine responses. Nat Rev Mater, 1–22 (2021).
27. Moyer TJ, Kato Y, Abraham W, Chang JYH, Kulp DW, Watson N, Turner HL, Menis S, Abbott RK, Bhiman JN, Melo MB, Simon HA, la Mata SH-D, Liang S, Seumois G, Agarwal Y, Li N, Burton DR, Ward AB, Schief WR, Crotty S, Irvine DJ, Engineered immunogen binding to alum adjuvant enhances humoral immunity. Nat Med 26, 430–440 (2020). [PubMed: 32066977]
28. Garcea RL, Meinerz NM, Dong M, Funke H, Ghazvini S, Randolph TW, Single-administration, thermostable human papillomavirus vaccines prepared with atomic layer deposition technology. Npj Vaccines 5, 45 (2020). [PubMed: 32528733]
29. Steichen JM, Lin Y-C, Havenar-Daughton C, Pecetta S, Ozorowski G, Willis JR, Toy L, Sok D, Liguori A, Kratochvil S, Torres JL, Kalyuzhniy O, Melzi E, Kulp DW, Raemisch S, Hu X, Bernard SM, Georgeson E, Phelps N, Adachi Y, Kubitz M, Landais E, Umotoy J, Robinson A, Briney B, Wilson IA, Burton DR, Ward AB, Crotty S, Batista FD, Schief WR, A generalized HIV vaccine design strategy for priming of broadly neutralizing antibody responses. Science 366, eaax4380 (2019). [PubMed: 31672916]
30. Silva M, Kato Y, Melo MB, Phung I, Freeman BL, Li Z, Roh K, Wijnbergen JWV, Watkins H, Enemuo CA, Hartwell BL, Chang JYH, Xiao S, Rodrigues KA, Cirelli KM, Li N, Haupt S, Aung A, Cossette B, Abraham W, Kataria S, Bastidas R, Bhiman J, Linde C, Bloom NI, Groschel B, Georgeson E, Phelps N, Thomas A, Bals J, Carnathan DG, Lingwood D, Burton DR, Alter G, Padera TP, Belcher AM, Schief WR, Silvestri G, Ruprecht RM, Crotty S, Irvine DJ, A particulate saponin/TLR agonist vaccine adjuvant alters lymph flow and modulates adaptive immunity. Sci Immunol 6, eabf1152 (2021). [PubMed: 34860581]
31. Rodrigues KA, Rodriguez-Aponte SA, Dalvie NC, Lee JH, Abraham W, Carnathan DG, Jimenez LE, Ngo JT, Chang JYH, Zhang Z, Yu J, Chang A, Nakao C, Goodwin B, Naranjo CA, Zhang L, Silva M, Barouch DH, Silvestri G, Crotty S, Love JC, Irvine DJ, Phosphate-mediated coanchoring of RBD immunogens and molecular adjuvants to alum potentiates humoral immunity against SARS-CoV-2. Sci Adv 7, eabj6538 (2021). [PubMed: 34878851]

32. Havenar-Daughton C, Carnathan DG, de la Peña AT, Pauthner M, Briney B, Reiss SM, Wood JS, Kaushik K, van Gils MJ, Rosales SL, van der Woude P, Locci M, Le KM, de Taeye SW, Sok D, Mohammed AUR, Huang J, Gumber S, Garcia A, Kasturi SP, Pulendran B, Moore JP, Ahmed R, Seumois G, Burton DR, Sanders RW, Silvestri G, Crotty S, Direct Probing of Germinal Center Responses Reveals Immunological Features and Bottlenecks for Neutralizing Antibody Responses to HIV Env Trimer. Cell Reports 17, 2195–2209 (2016). [PubMed: 27880897]
33. Baumjohann D, Preite S, Reboldi A, Ronchi F, Ansel KM, Lanzavecchia A, Sallusto F, Persistent Antigen and Germinal Center B Cells Sustain T Follicular Helper Cell Responses and Phenotype. Immunity 38, 596–605 (2013). [PubMed: 23499493]
34. Mintz MA, Cyster JG, T follicular helper cells in germinal center B cell selection and lymphomagenesis. Immunol Rev 296, 48–61 (2020). [PubMed: 32412663]
35. Yang L, Beek MV, Wang Z, Muecksch F, Canis M, Hatziioannou T, Bieniasz PD, Nussenzweig MC, Chakraborty AK, Antigen presentation dynamics shape the antibody response to variants like SARS-CoV-2 Omicron after multiple vaccinations with the original strain. Cell Reports 42, 112256 (2022).
36. Pulendran B, Arunachalam PS, O'Hagan DT, Emerging concepts in the science of vaccine adjuvants. Nat Rev Drug Discov, 1–22 (2021). [PubMed: 33097914]
37. Mayer A, Zhang Y, Perelson AS, Wingreen NS, Regulation of T cell expansion by antigen presentation dynamics. Proc National Acad Sci 116, 5914–5919 (2019).
38. Johansen P, Storni T, Rettig L, Qiu Z, Der-Sarkissian A, Smith KA, Manolova V, Lang KS, Senti G, Müllhaupt B, Gerlach T, Speck RF, Bot A, Kündig TM, Antigen kinetics determines immune reactivity. Proc National Acad Sci 105, 5189–5194 (2008).
39. Quiel J, Caucheteux S, Laurence A, Singh NJ, Bocharov G, Ben-Sasson SZ, Grossman Z, Paul WE, Antigen-stimulated CD4 T-cell expansion is inversely and log-linearly related to precursor number. Proc National Acad Sci 108, 3312–3317 (2011).
40. Aung A, Cui A, Maiorino L, Amini AP, Gregory JR, Bukenya M, Zhang Y, Lee H, Cottrell CA, Morgan DM, Silva M, Suh H, Kirkpatrick JD, Amlashi P, Remba T, Froehle LM, Xiao S, Abraham W, Adams J, Love JC, Huyett P, Kwon DS, Hacohen N, Schief WR, Bhatia SN, Irvine DJ, Low protease activity in B cell follicles promotes retention of intact antigens after immunization. Science 379, eabn8934 (2023). [PubMed: 36701450]
41. Phan TG, Grigorova I, Okada T, Cyster JG, Subcapsular encounter and complement-dependent transport of immune complexes by lymph node B cells. Nat. Immunol. 8, 992–1000 (2007). [PubMed: 17660822]
42. Phan TG, Green JA, Gray EE, Xu Y, Cyster JG, Immune complex relay by subcapsular sinus macrophages and noncognate B cells drives antibody affinity maturation. Nat Immunol 10, 786–793 (2009). [PubMed: 19503106]
43. Ferguson AR, Youd ME, Corley RB, Marginal zone B cells transport and deposit IgM-containing immune complexes onto follicular dendritic cells. Int. Immunol 16, 1411–1422 (2004). [PubMed: 15326094]
44. Kulp DW, Steichen JM, Pauthner M, Hu X, Schiffner T, Liguori A, Cottrell CA, Havenar-Daughton C, Ozorowski G, Georgeson E, Kalyuzhniy O, Willis JR, Kubitz M, Adachi Y, Reiss SM, Shin M, de Val N, Ward AB, Crotty S, Burton DR, Schief WR, Structure-based design of native-like HIV-1 envelope trimers to silence non-neutralizing epitopes and eliminate CD4 binding. Nat Commun 8, 1655 (2017). [PubMed: 29162799]
45. Rodrigues KA, Cottrell CA, Steichen JM, Groschel B, Abraham W, Suh H, Agarwal Y, Ni K, Chang JYH, Yousefpour P, Melo MB, Schief WR, Irvine DJ, Optimization of an alum-anchored clinical HIV vaccine candidate. npj Vaccines 8, 117 (2023). [PubMed: 37573422]
46. Qi H, T follicular helper cells in space-time. Nat Rev Immunol 16, 612–625 (2016). [PubMed: 27573485]
47. Crotty S, T Follicular Helper Cell Differentiation, Function, and Roles in Disease. Immunity 41, 529–542 (2014). [PubMed: 25367570]
48. Crotty S, T Follicular Helper Cell Biology: A Decade of Discovery and Diseases. Immunity 50, 1132–1148 (2019). [PubMed: 31117010]

49. Devarajan P, Vong AM, Castonguay CH, Kugler-Umana O, Bautista BL, Jones MC, Kelly KA, Xia J, Swain SL, Strong influenza-induced TFH generation requires CD4 effectors to recognize antigen locally and receive signals from continuing infection. Proc National Acad Sci 119, e2111064119 (2022).
50. Deenick EK, Chan A, Ma CS, Gatto D, Schwartzberg PL, Brink R, Tangye SG, Follicular Helper T Cell Differentiation Requires Continuous Antigen Presentation that Is Independent of Unique B Cell Signaling. Immunity 33, 241–253 (2010). [PubMed: 20691615]
51. Kelly HG, Tan H-X, Juno JA, Esterbauer R, Ju Y, Jiang W, Wimmer VC, Duckworth BC, Groom JR, Caruso F, Kanekiyo M, Kent SJ, Wheatley AK, Self-assembling influenza nanoparticle vaccines drive extended germinal center activity and memory B cell maturation. JCI Insight 5, e136653 (2020). [PubMed: 32434990]
52. Dominguez-Sola D, Victora GD, Ying CY, Phan RT, Saito M, Nussenzweig MC, Dalla-Favera R, The proto-oncogene MYC is required for selection in the germinal center and cyclic reentry. Nat Immunol 13, 1083–1091 (2012). [PubMed: 23001145]
53. Shulman Z, Gitlin AD, Targ S, Jankovic M, Pasqual G, Nussenzweig MC, Victora GD, T Follicular Helper Cell Dynamics in Germinal Centers. Science 341, 673–677 (2013). [PubMed: 23887872]
54. Cirelli KM, Crotty S, Germinal center enhancement by extended antigen availability. Curr Opin Immunol 47, 64–69 (2017). [PubMed: 28738289]
55. Hu JK, Crampton JC, Cupo A, Ketas T, van Gils MJ, Sliepen K, de Taeye SW, Sok D, Ozorowski G, Deresa I, Stanfield R, Ward AB, Burton DR, Klasse PJ, Sanders RW, Moore JP, Crotty S, Murine Antibody Responses to Cleaved Soluble HIV-1 Envelope Trimers Are Highly Restricted in Specificity. J Virol 89, 10383–10398 (2015). [PubMed: 26246566]
56. McHugh KJ, Nguyen TD, Linehan AR, Yang D, Behrens AM, Rose S, Tochka ZL, Tzeng SY, Norman JJ, Anselmo AC, Xu X, Tomasic S, Taylor MA, Lu J, Guarecuco R, Langer R, Jaklenec A, Fabrication of fillable microparticles and other complex 3D microstructures. Science 357, 1138–1142 (2017). [PubMed: 28912242]
57. Steichen JM, Kulp DW, Tokatlian T, Escolano A, Dosenovic P, Stanfield RL, McCoy LE, Ozorowski G, Hu X, Kalyuzhniy O, Briney B, Schiffner T, Garces F, Freund NT, Gitlin AD, Menis S, Georgeson E, Kubitz M, Adachi Y, Jones M, Mutafyan AA, Yun DS, Mayer CT, Ward AB, Burton DR, Wilson IA, Irvine DJ, Nussenzweig MC, Schief WR, HIV Vaccine Design to Target Germline Precursors of Glycan-Dependent Broadly Neutralizing Antibodies. Immunity 45, 483–496 (2016). [PubMed: 27617678]
58. Tokatlian T, Read BJ, Jones CA, Kulp DW, Menis S, Chang JYH, Steichen JM, Kumari S, Allen JD, Dane EL, Liguori A, Sangesland M, Lingwood D, Crispin M, Schief WR, Irvine DJ, Innate immune recognition of glycans targets HIV nanoparticle immunogens to germinal centers. Science 363, 649–654 (2019). [PubMed: 30573546]
59. Didierlaurent AM, Morel S, Lockman L, Giannini SL, Bisteau M, Carlsen H, Kielland A, Vosters O, Vanderheyde N, Schiavetti F, Larocque D, Mechelen MV, Garçon N, AS04, an aluminum salt- and TLR4 agonist-based adjuvant system, induces a transient localized innate immune response leading to enhanced adaptive immunity. J. Immunol. (Baltim., Md : 1950) 183, 6186–97 (2009).
60. Dupuis M, McDonald DM, Ott G, Distribution of adjuvant MF59 and antigen gD2 after intramuscular injection in mice. Vaccine 18, 434–439 (1999). [PubMed: 10519932]
61. Murphy K, Weaver C, Janeway's Immunobiology. doi: 10.1201/9781315533247 (2016).
62. Awate S, Babiuk LA, Mutwiri G, Mechanisms of Action of Adjuvants. Front. Immunol 4, 114 (2013). [PubMed: 23720661]
63. Liang F, Lindgren G, Sandgren KJ, Thompson EA, Francica JR, Seubert A, Gregorio ED, Barnett S, O'Hagan DT, Sullivan NJ, Koup RA, Seder RA, Loré K, Vaccine priming is restricted to draining lymph nodes and controlled by adjuvant-mediated antigen uptake. Sci. Transl. Med 9 (2017).
64. Calabro S, Tortoli M, Baudner BC, Pacitto A, Cortese M, O'Hagan DT, Gregorio ED, Seubert A, Wack A, Vaccine adjuvants alum and MF59 induce rapid recruitment of neutrophils and monocytes that participate in antigen transport to draining lymph nodes. Vaccine 29, 1812–1823 (2011). [PubMed: 21215831]

65. Altan-Bonnet G, Mora T, Walczak AM, Quantitative immunology for physicists. Phys. Rep 849, 1–83 (2020).

66. Okada T, Miller MJ, Parker I, Krummel MF, Neighbors M, Hartley SB, O'Garra A, Cahalan MD, Cyster JG, Antigen-Engaged B Cells Undergo Chemotaxis toward the T Zone and Form Motile Conjugates with Helper T Cells. PLoS Biol. 3, e150 (2005). [PubMed: 15857154]

67. Taylor JJ, Pape KA, Steach HR, Jenkins MK, Apoptosis and antigen affinity limit effector cell differentiation of a single naïve B cell. Science 347, 784–787 (2015). [PubMed: 25636798]

68. Sze DM-Y, Toellner K-M, de Vinuesa CG, Taylor DR, MacLennan ICM, Intrinsic Constraint on Plasmablast Growth and Extrinsic Limits of Plasma Cell Survival. J. Exp. Med 192, 813–822 (2000). [PubMed: 10993912]

69. Moran I, Nguyen A, Khoo WH, Butt D, Bourne K, Young C, Hermes JR, Biro M, Gracie G, Ma CS, Munier CML, Luciani F, Zaunders J, Parker A, Kelleher AD, Tangye SG, Croucher PI, Brink R, Read MN, Phan TG, Memory B cells are reactivated in subcapsular proliferative foci of lymph nodes. Nat. Commun 9, 3372 (2018). [PubMed: 30135429]

70. Beek MV, Nussenzweig MC, Chakraborty AK, Two complementary features of humoral immune memory confer protection against the same or variant antigens. Proc. Natl. Acad. Sci 119, e2205598119 (2022). [PubMed: 36006981]

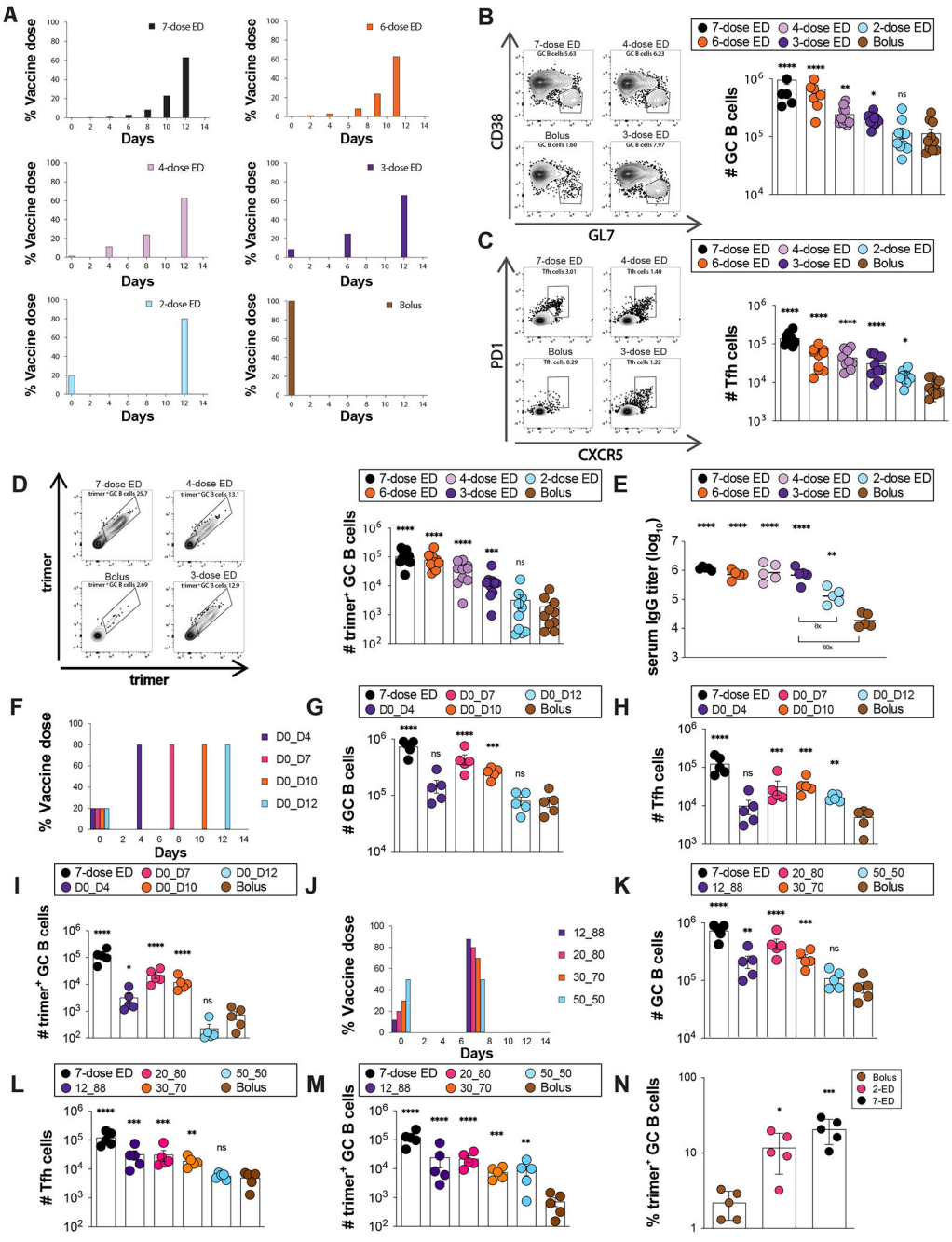

Figure 1. An optimally designed two-shot extended-prime vaccination substantially enhances GC responses to subunit vaccines compared to bolus immunization.

(A) Schematic of escalating dose vaccination regimens with varying dose number. (**B-E**) C57BL/6J mice (*n*=10 animals/group) were immunized with 10 μg N332-GT2 trimer and 5 μg SMNP adjuvant according to the dosing schemes in (**A**). GC responses were evaluated on day 14 by flow cytometry and antibody responses by ELISA on day 28. Shown are representative flow cytometry histograms and cell counts for total GC B cells (**B**), Tfh (**C**), and trimer-specific GC B cells (**D**) at day 14, and trimer-specific serum IgG titers at day 28 (**E**). (**F**) Schematic of dosing schedules tested for two-shot ED regimens. (**G-I**)

C57BL/6J mice (*n*=5 animals/group) were immunized with 10 μg N332-GT2 trimer and 5 μg SMNP adjuvant according to the dosing schemes in (**F**), and total GC B cells (**G**), Tfh cells (**H**), and trimer-specific GC B cells (**I**) were analyzed by flow cytometry on day 14. Note: Bolus and 7-dose ED comparisons are also shown with black and brown colors respectively. (**J**) Schematic of dosing ratios evaluted for for 2-shot ED immunization. (**I-M**) C57BL/6J mice (*n*=5 animals/group) were immunized with 10 μg N332-GT2 trimer and 5 μg SMNP adjuvant according to the dosing schemes in (**J**), and total GC B cells (**K**), Tfh cells (**L**), and trimer-specific GC B cells (**M**) were analyzed by flow cytometry on day 14. (**N**) Frequencies of GC B cells recognizing intact trimer antigen for bolus, optimized 2-ED, and 7-ED regimens. Points represent responses of individual animals while bars indicate mean± s.e.m. Shown are data from one representative of two independent experiments for each immunization series. ****, $p < 0.0001$; ***, $p < 0.001$; **, $p < 0.01$; *, $p < 0.05$; ns, not significant; by one-way ANOVA with Dunnett's multiple comparison post test compared to bolus immunization.

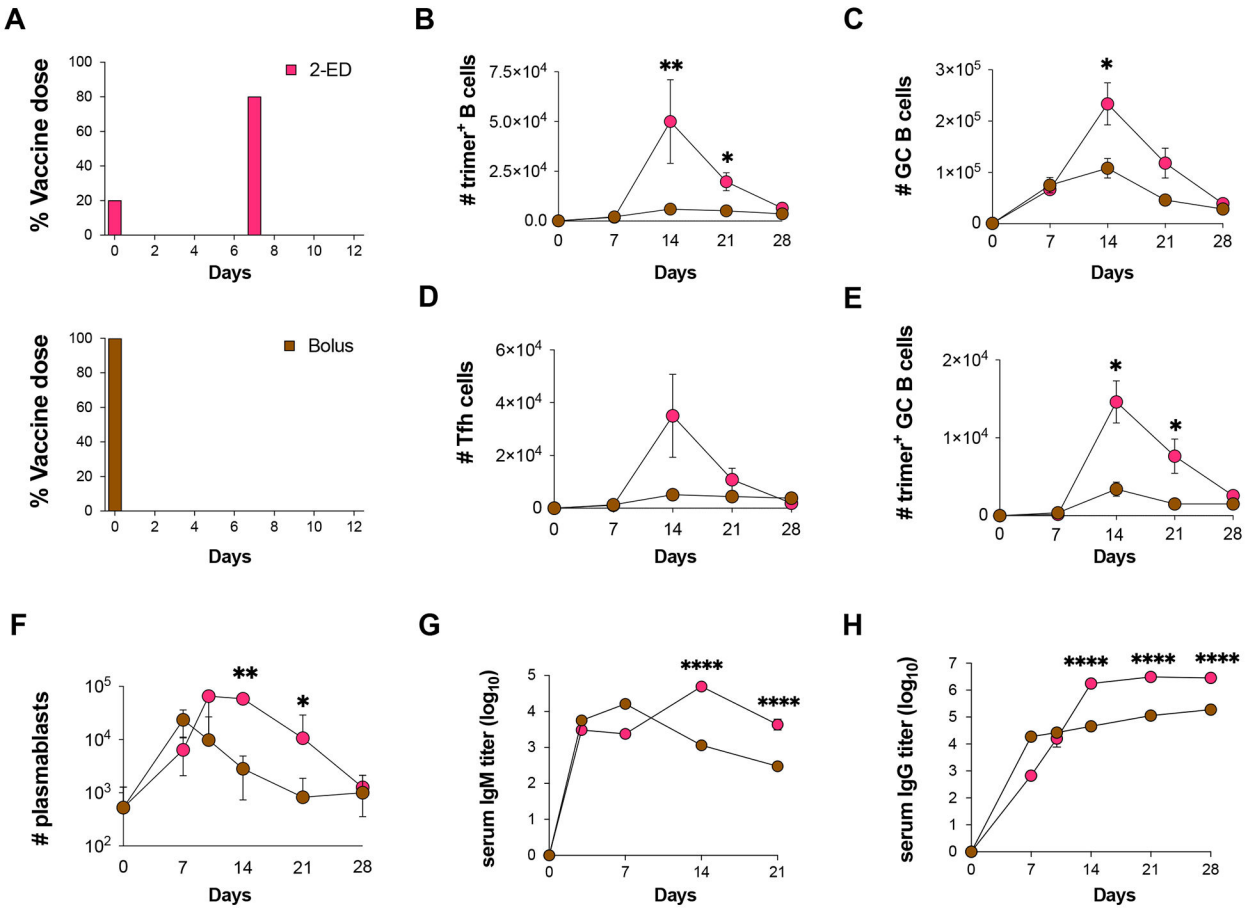

Figure 2. Optimized 2-shot prime immunization amplifies the GC response and trimer-specific serum antibody titers over time compared to bolus immunization.

(**A**) Schematic of dosing schemes. (**B-H**) C57BL/6J mice (*n*=9 animals/group) were immunized with 10 μg N332-GT2 trimer and 5 μg SMNP adjuvant according to the dosing schemes in (**A**). GC responses were evaluated on days 7, 14, 21, and 28 by flow cytometry and antibody responses by ELISA on days 3, 7, 14, 21, and 28. Shown are trimer-specific B cell counts (**B**), GC B cell counts (**C**), Tfh cell counts (**D**), trimer-specific GC B cell counts (**E**), plasmablast counts (**F**), trimer-specific IgM titers (**G**), and trimer-specifc IgG titers (**H**), plotted over time for bolus and 2-ED regimens. Shown are data from one independent experiment for each immunization series. ****, $p < 0.0001$; ***, $p < 0.001$; **, $p < 0.01$; *, $p < 0.05$; ns, not significant; by two-way ANOVA with Dunnett's multiple comparison post test compared to bolus immunization.

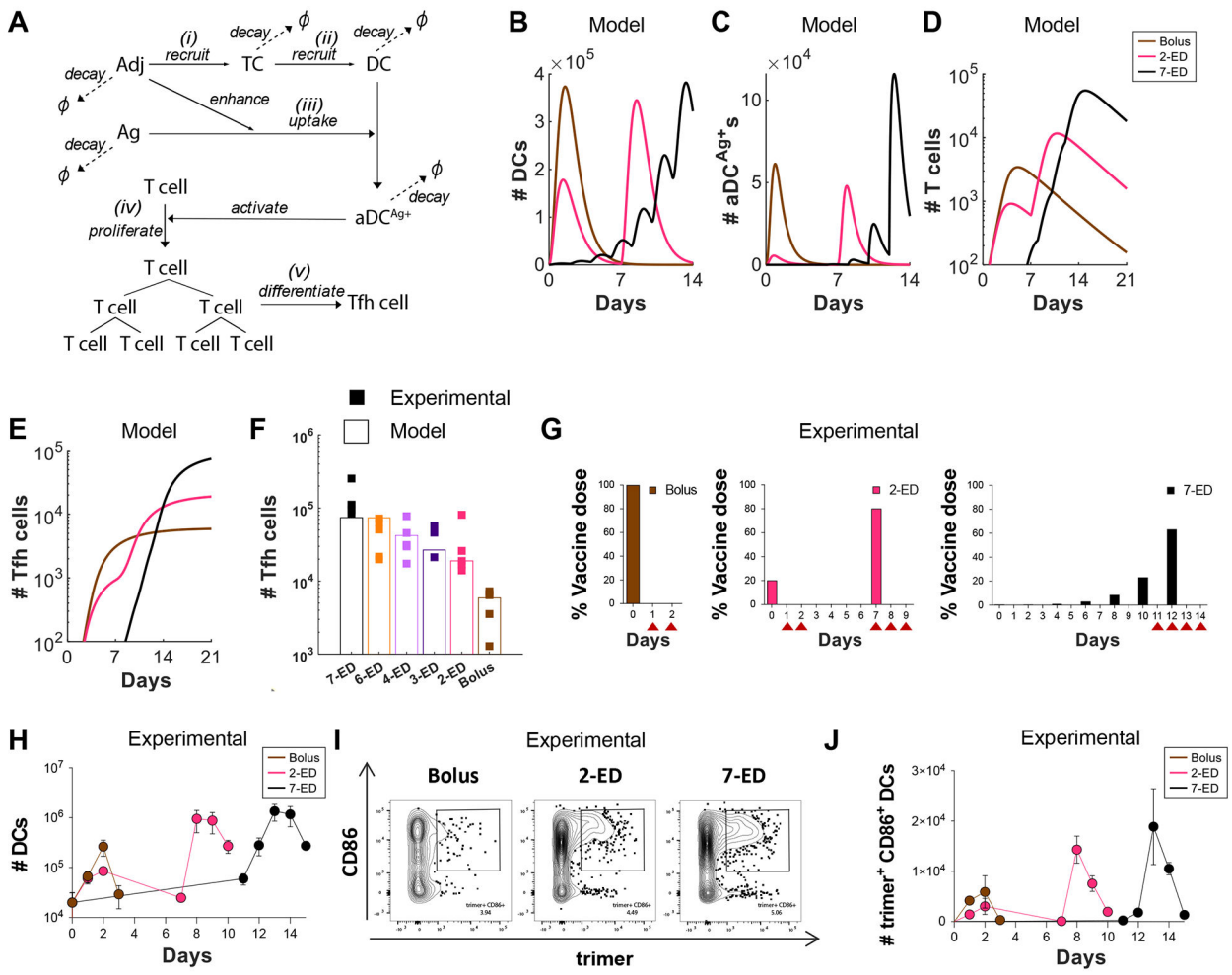

Figure 3. In Silico modeling predicts enhanced T cell priming with extended-prime immunization, consistent with experimental measurements of DC antigen acquisition and activation in draining lymph nodes.

(**A-F**) Computational model of vaccine uptake by dendritic cells and helper T cell priming. (**A**) Schematic outlining elements of the kinetic model. (**B-E**) Modeling predictions of the number of (**B**) total DCs (**B**), $Ag^{+}Adj^{+}$ DCs (**C**), Ag-specific T cells (**D**), and Tfh cells (**E**) for bolus, 2-ED, or 7-ED immunization regimens. (**F**) Comparing Tfh cell count predicted by the model with the experimental data at day 14. (**G-J**) Experimental analysis of lymph node DC antigen uptake and activation. C57BL/6J mice (n=3 animals/group) were immunized with 10 μg Cy5 dye-labled-N332-GT2 trimer and 5 μg SMNP adjuvant according to the dosing schemes shown in (**G),** and DCs in draining lymph nodes were analyzed by flow cytometry on days indicated by arrows. Shown are number of DCs (**H**), representative histograms of trimer antigen fluorescence and CD86 expression by $CD11c^{+}$ DCs (**I**), and number of $trimer^{+}CD86^{+}$ DC counts over time for bolus, 2-ED, and 7-ED immunization regimens (**J**).

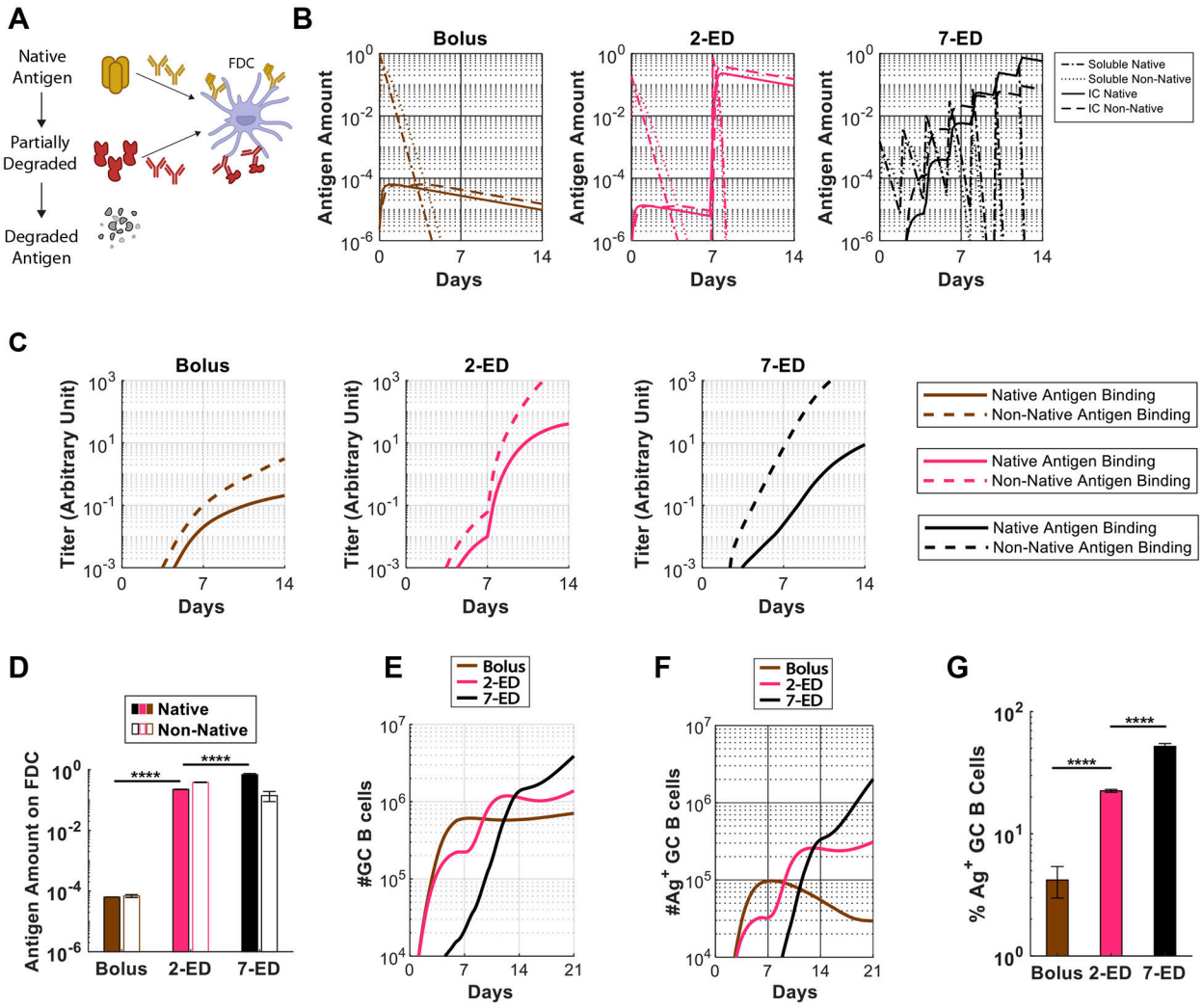

Figure 4. *In Silico* modeling predicts increased intact antigen accumulation on FDCs for extended dosing compared to bolus immunization.

(**A**) Schematic showing antigen fates considered in the computational model. (**B**) *In silico* prediction of the amount of free antigen in lymph nodes over time in an intact ("soluble native") or degraded ("soluble non-native") state, and amounts of native and non-native antigen captured on FDCs in the form of immune complexes ("IC") over time. The antigen amounts are normalized to the total antigen dose in immunization. (**C**) Antibody titers predicted by the *in silico* model for bolus, 2-ED, and 7-ED immunization regimens. In the simulation, antibody titers are defined as the concentration of antibodies weighted by their affinities, reflecting their capabilities to bind to the antigen. (**D**) Comparison of predicted antigen amounts accumulated on FDCs after the final shot from each dosing scheme, normalized to the total antigen dose in immunization. (**E**) Model prediction for the number of GC B cells over time. (**F, G**) Model prediction for the number of native antigen-binding (i.e. trimer^{+}) GC B cells over time (**F**) and frequency of trimer^{+} GC B cells at day 21 (**G**) from bolus, 2-ED, and 7-ED immunization schemes. The results reported are mean values from 10 independent stochastic simulations of the lymph node. ****, $p < 0.0001$; by one-way ANOVA with Tukey's multiple comparison post test.

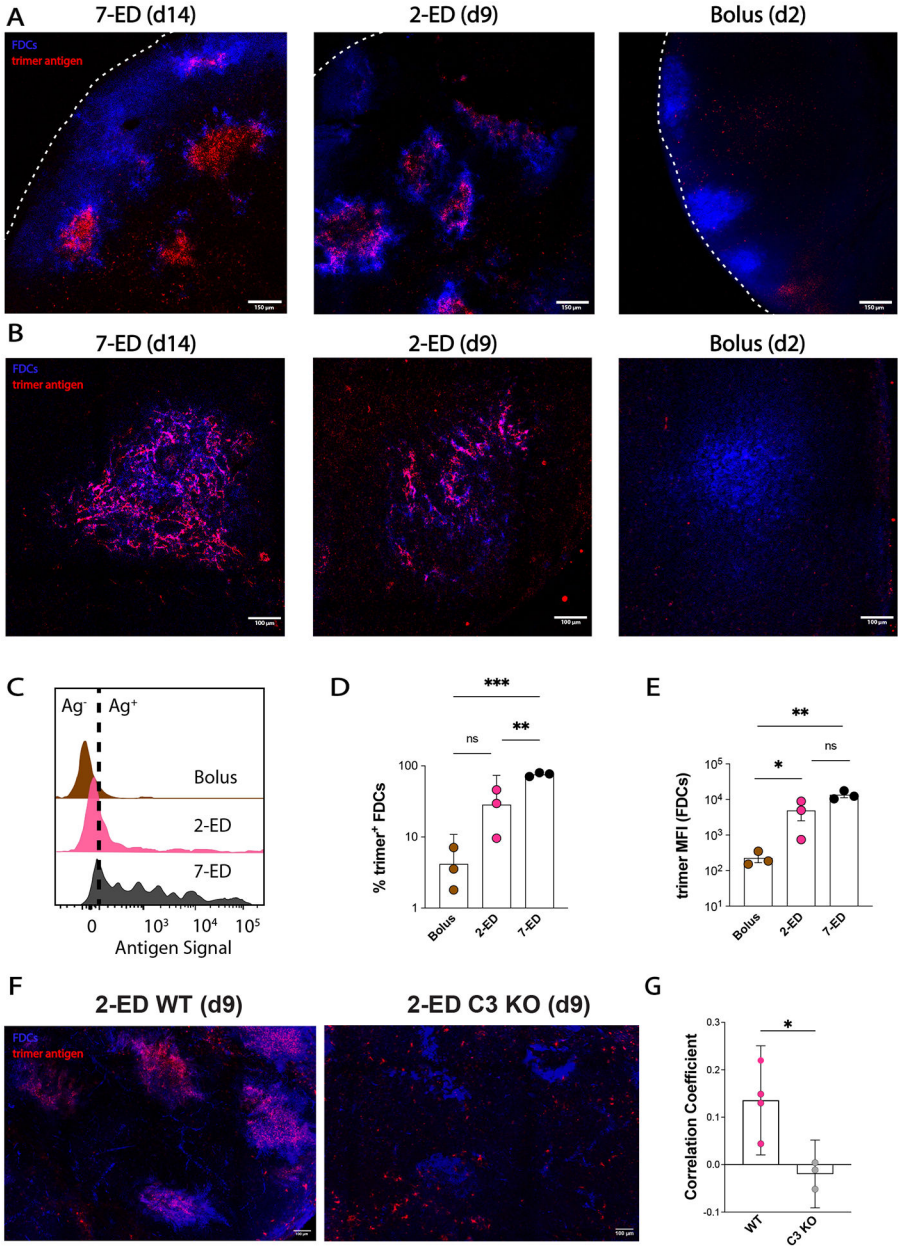

Figure 5. Two-dose extended prime immunization enables antigen capture of the second shot on FDCs.

(**A-B**) Groups of C57BL/6 mice (n=3 animals/group) were immunized by bolus, 2-ED, or 7-ED regimens as in Fig. 3G followed by collection of lymph nodes for imaging at 48 h after bolus or after the last injection of 2-ED and 7-ED regimens. FDC networks were labeled *in situ* by s.c. injection of anti-CD35 antibody 16h before tissue collection. Collected tissues were clarified and imaged intact by confocal microscopy; shown are maximum intensity projections from z-stacks through FDC clusters (Scale bars, 150 μm), (**A**). Alternatively, lymph node sections were stained for FDCs (CD35; blue) and then analyzed by confocal microscopy (Scale bars, 300 μm) to detect co-localization with Cy5-labeled N332-GT2 (pink), (**B**). (**C-E**) Flow cytometry analysis of LN cells (*n*=3 pools/group,

with each pool containing six LNs from 3 mice) isolated 48 hr after the final injection following immunization with fluorescently labeled N332-GT2 (10 ug) and SMNP (5 ug) using either bolus, 2-ED, or 7-ED dosing regimens. Shown are representative histograms of antigen intensities among LN cells (**C**), frequencies of trimer+ FDCs (**D**), and the mean trimer fluorescence intensity among trimer^{+} FDCs (**E**) for the indicated immunization conditions. Shown are data from one independent experiment for each immunization series. (**F-G**) C57BL/6 WT and complement-deficient (C3 knockout) mice (n=3-4 animals/group) were immunized by 2-ED regimen with Cy5-labeled antigen followed by collection of lymph nodes for imaging 48h later. BV421-tagged anti-CD35 was injected 16h prior to tissue collection for FDC labeling. Collected tissues were clarified and imaged intact by confocal microscopy. **(F)** Maximum intensity projections from z-stacks of WT (left) and C3 knockout (right) mice (Scale bars, 100 um). (**G)** Quantification of N332:anti-CD35 signal colocalization as determined by Pearson's correlation. ****, $p < 0.0001$; ***, $p < 0.001$; **, $p < 0.01$; *, $p < 0.05$; ns, not significant; by one-way ANOVA with Dunnett’s multiple comparison post test compared to bolus immunization.

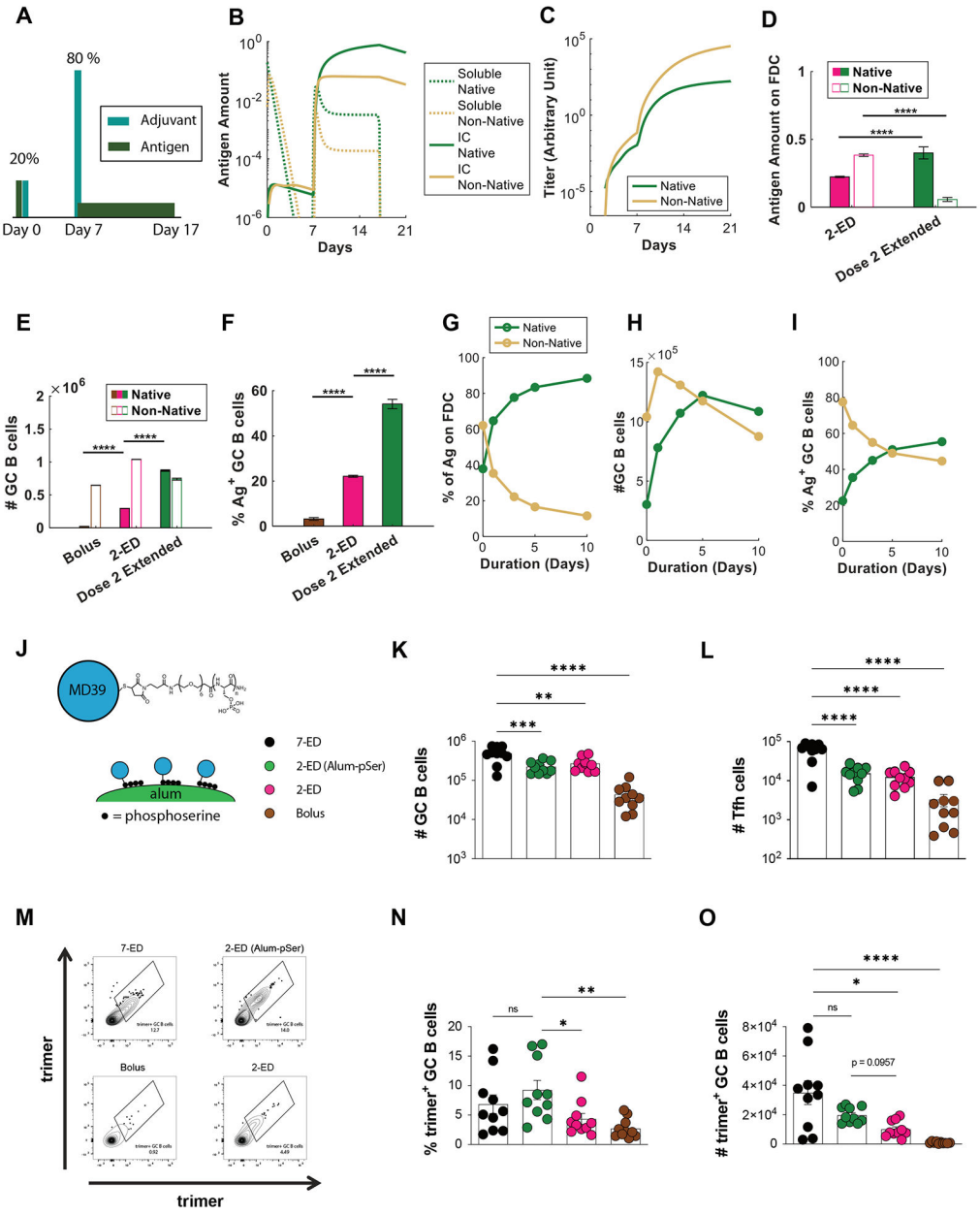

Figure 6. Extending the duration of antigen delivery during the second dose of 2-ED vaccination increases native antigen capture on FDCs and antigen-specific GC responses.

(**A-I**) Computational modeling of GC responses elicited by 2-ED dosing administered as two bolus doses vs. a bolus on day 0 and a prolonged antigen delivery at day 7 ("dose 2 extended"). (**A**) Schematic of 2-ED vs. "dose 2 extended" vaccination regimens. (**B, C**) Amounts of free and immune-complexed native or degraded ("non-native") antigen in the LN over time (**B**) and serum antibody titers recognizing native vs. non-native antigen (**C**) for the "dose 2 extended" regimen. (**D-F**) *In silico* prediction of antigen captured on FDCs (**D**), total GC B cells at day 21 (**E**), and frequency of trimer-binding GC B cells at day 21 (**F**) for bolus, 2-ED, and "dose 2 extended" vaccination regimens. (**G-I**) *In silico* prediction of proportions of intact vs. degraded antigen captured by FDCs (**G**), total number of GC

B cells (**H**), and the fraction of GC B cells that are native vs. non-native antigen-binding (**I**) at day 21 as a function of the duration of antigen release used in “dose 2 extended” vaccination. (**J-O**) Experimental testing of “dose 2 extended” immunizations using alum-anchored immunogens. (**J**) Schematic demonstrating anchoring trimer immunogen onto alum via phosphoserine linkers (Alum-pSer). (**K-O**) C57BL/6J mice (n=10 animals/group) were immunized with 10 μg MD39 trimer (either soluble bound to 50 μg alum) and 5 μg SMNP adjuvant as in Fig. 3G. Shown are the numbers of GC B cells (**K**) and Tfh cells (**L**), representative histograms of trimer staining of GC B cells (**M**), frequencies of trimer-binding GC B cells (**N**), and the number of trimer-binding GC B cells (**O**), for the different dosing regimens determined by flow cytometry at day 14. Shown are data from one representative of two independent experiments for each immunization series. ****, $p < 0.0001$; ***, $p < 0.001$; **, $p < 0.01$; *, $p < 0.05$; ns, not significant; by one-way ANOVA with Dunnett’s multiple comparison post test compared to bolus immunization.